

1 **Marine Carbohydrates and Other Sea Spray Aerosol Constituents Across**  
2 **Altitudes in the Lower Troposphere of Ny-Ålesund, Svalbard**

3 **Sebastian Zeppenfeld<sup>1\*</sup>, Jonas Schaefer<sup>2</sup>, Christian Pilz<sup>2</sup>, Kerstin Ebell<sup>3</sup>, Moritz Zeising<sup>4</sup>, Frank**  
4 **Stratmann<sup>2</sup>, Holger Siebert<sup>2</sup>, Birgit Wehner<sup>2</sup>, Matthias Wietz<sup>4,5,6</sup>, Astrid Bracher<sup>4,7</sup>, and**  
5 **Manuela van Pinxteren<sup>1</sup>**

6 1 Atmospheric Chemistry Department (ACD), Leibniz Institute for Tropospheric Research (TROPOS),  
7 Leipzig, Germany

8 2 Atmospheric Microphysics (AMP), Leibniz Institute for Tropospheric Research (TROPOS), Leipzig,  
9 Germany

10 3 Institute for Geophysics and Meteorology, University of Cologne, Cologne, Germany

11 4 Alfred Wegener Institute Helmholtz Centre for Polar and Marine Research, Bremerhaven, Germany

12 5 Max Planck Institute for Marine Microbiology, Bremen, Germany

13 6 Institute for Chemistry and Biology of the Marine Environment, University of Oldenburg, Oldenburg,  
14 Germany

15 7 Institute of Environmental Physics, University of Bremen, Bremen, Germany

16

17 \*Correspondence to: Sebastian Zeppenfeld (zeppenfeld@tropos.de)

18

19

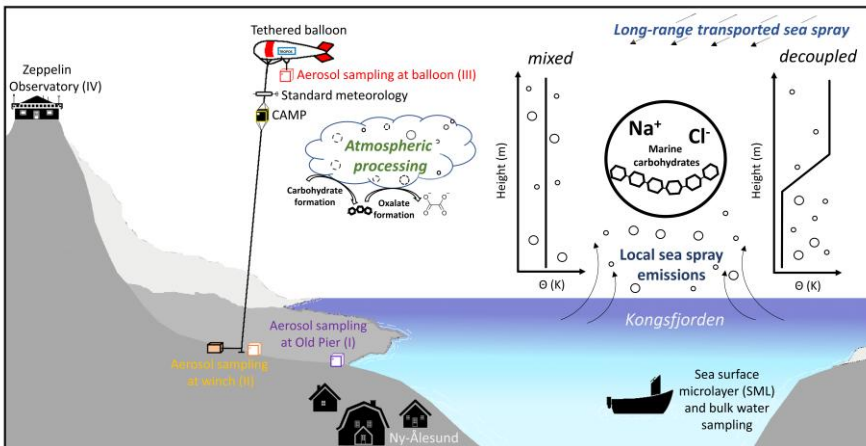
20 **Abstract**

21 Marine combined carbohydrates in aerosol particles (CCHO<sub>aer</sub>) have the potential to influence  
22 cloud formation and properties, but it remains unclear to what extent they reach altitudes  
23 relevant for cloud processes. Balloon-borne measurements of major sea spray aerosol (SSA)  
24 constituents, including sodium (Na<sup>+</sup><sub>aer</sub>) and CCHO<sub>aer</sub>, were conducted in autumn 2021 and  
25 spring 2022 in Ny-Ålesund (Svalbard). Total suspended particles were collected at 321–1112 m,  
26 covering both the marine boundary layer and the free troposphere, with Na<sup>+</sup><sub>aer</sub> ranging 23–  
27 850 ng m<sup>-3</sup> and CCHO<sub>aer</sub> 3.8–274 ng m<sup>-3</sup>. The chemical composition of balloon-borne aerosol  
28 samples was compared with synchronized ground level measurements at the balloon's winch  
29 (Na<sup>+</sup><sub>aer</sub>: 35–3710 ng m<sup>-3</sup>; CCHO<sub>aer</sub>: 1.9–194 ng m<sup>-3</sup>), and at the Old Pier (Na<sup>+</sup><sub>aer</sub>: 140–1470 ng m<sup>-3</sup>;  
30 CCHO<sub>aer</sub>: 1.6–10.0 ng m<sup>-3</sup>), where freshly emitted SSA particles were sampled. Surface  
31 seawater from the Kongsfjorden was analyzed to evaluate the sea-air transfer of marine  
32 CCHO. Air mass histories, atmospheric mixing, and cloud conditions were evaluated for three  
33 selected cases to explain vertical concentration patterns. A strong correlation (R=0.78,  
34 p<0.001) between combined xylose (<0.2–14.1 ng m<sup>-3</sup>) in CCHO<sub>aer</sub> and oxalate<sub>aer</sub> (<1–67 ng m<sup>-3</sup>)  
35 across all altitudes, suggests either coproduction or a connection through atmospheric

36 processing. These results provide a first comprehensive picture of local primary sea-air  
37 transfer of marine combined carbohydrates and highlight the roles of long-range transport,  
38 in-situ formation, and atmospheric processing in shaping their distribution.

39

40



41

## 42 1. Introduction

43 Aerosol particles in the High Arctic atmosphere originate from a complex interplay of primary  
44 and secondary emissions from oceanic, terrestrial, cryospheric, and anthropogenic sources,  
45 followed by diverse atmospheric processes (Schmale et al., 2021). They play a crucial role in  
46 the radiation balance, directly by scattering and absorbing shortwave and longwave radiation,  
47 and indirectly by influencing cloud formation and phase state as cloud condensation nuclei  
48 and ice-nucleating particles (Lohmann and Feichter, 2005; Penner et al., 2001; Quinn et al.,  
49 2015; Yu et al., 2006). These effects are strongly governed by the particles' size distribution  
50 and chemical composition (Dusek et al., 2006; Farmer et al., 2015; Kanji et al., 2017; Pilinis et  
51 al., 1995).

52 The High Arctic predominantly consists of marine areas, characterized by a seasonally variable  
53 extent of sea ice cover and open waters. Consequently, sea spray aerosol (SSA) particles  
54 represent a key group of primary aerosol particles in this region (Heutte et al., 2025; Kang et  
55 al., 2025; Schmale et al., 2022). As Arctic sea ice coverage continues to decline due to global  
56 warming, enhanced by Arctic amplification (Cai et al., 2021; Francis and Wu, 2020; Wendisch  
57 et al., 2017, 2023), larger expanses of open ocean are anticipated to become significant  
58 sources of SSA emissions (Browse et al., 2014; Struthers et al., 2011). Although direct  
59 measurements remain sparse, Sharma et al. (2019) readily observed increasing sea salt  
60 aerosol production from sea spray over 34 years at the Arctic air chemistry observatory in  
61 Alert, Canada.

62 SSA particles are generated through wind-driven wave action, which causes bubbles at the sea  
63 surface to burst, ejecting film and jet droplets into the atmosphere (Veron, 2015). SSA  
64 particles primarily consist of inorganic sea salt ions, mainly sodium and chloride, along with  
65 organic matter (OM), including significant amounts of marine carbohydrates originating from  
66 the sea surface microlayer (SML) and the underlying bulk seawater (Müller et al., 2010; van  
67 Pinxteren et al., 2023; Quinn et al., 2015; Russell et al., 2010). In seawater, carbohydrates are  
68 produced by photoautotrophic organisms, predominantly as linear or branched oligo- and  
69 polysaccharides (Aluwihare et al., 1997; Borch and Kirchman, 1997; Engel and Händel, 2011;  
70 Khadem, 2012), collectively referred to as combined carbohydrates (CCHO). They also exist as  
71 monosaccharides, known as dissolved free carbohydrates (~~DFCHO~~). Both ~~fractions DFCHO and~~  
72 ~~CCHO~~ are consumed or transformed by heterotrophic organisms, with turnover rates largely

73 determined by their molecular structure and composition ~~of the carbohydrates~~ (Arnosti et al.,  
74 2021; Engel and Händel, 2011; Ittekkot et al., 1981; Kirchman et al., 2001).

75 Sodium in aerosol particles ( $\text{Na}^+_{\text{aer}}$ ) is highly abundant in the marine boundary layer, with only  
76 minor terrestrial sources and greater atmospheric stability compared to chloride ( $\text{Cl}^-_{\text{aer}}$ ) (Chi  
77 et al., 2015; Keene et al., 1986; Manders et al., 2010; Sander et al., 2003). This makes it a  
78 valuable conservative tracer for studying the sea-to-air transfer and atmospheric  
79 transformation of organic compounds, including marine carbohydrates, as well as other  
80 inorganic SSA constituents. Notably, the ratio of OM to  $\text{Na}^+$  is significantly higher in SSA  
81 particles than in seawater, reflecting not only the preferential enrichment of surface-active  
82 substances at the interface but also a more complex interplay of factors such as water  
83 solubility, biological activity within the ocean surface, and co-adsorption processes involving  
84 matrix constituents (Burrows et al., 2014; Gantt et al., 2011; Hasenecz et al., 2020, 2019;  
85 Hoffman and Duce, 1976; Jayarathne et al., 2016; van Pinxteren et al., 2017; Quinn et al., 2015;  
86 Russell et al., 2010; Schill et al., 2018). This enrichment is particularly pronounced in  
87 submicron particles compared to supermicron particles. Furthermore, following the sea-to-air  
88 transfer of OM and CCHO, recent laboratory (Hasenecz et al., 2020; Malfatti et al., 2019) and  
89 field (Zeppenfeld et al., 2021, 2023) observations suggest their molecular transformation or  
90 additional in-situ formation, driven by abiotic, microbial or enzymatic activities in the  
91 atmosphere.

92 SSA particles are known to function as both cloud condensation nuclei (Orellana et al., 2011;  
93 Xu et al., 2022) and ice-nucleating particles (Alpert et al., 2022; DeMott et al., 2016; Hill et al.,  
94 2023; Mirrielees et al., 2024), underscoring their important role in cloud microphysics, cloud  
95 formation, and precipitation processes. Recently, Hartmann et al. (2025) demonstrated,  
96 through a combination of lab and field data, that SSA particles' ice-nucleating activity is likely  
97 attributable to the polysaccharides they contain. Model simulations further indicated that the  
98 ice-nucleating activity of marine polysaccharides is particularly significant within the  
99 temperature range between  $-20$  and  $-15^\circ\text{C}$  in remote oceanic regions, where contributions  
100 from terrestrial ice-nucleating particles are minimal or absent. Furthermore, Rocchi et al.,  
101 (2024) demonstrated that the presence of glucose-rich CCHO, in combination with sea salt,  
102 significantly enhances SSA production in eastern Arctic waters. This finding may improve the  
103 predictability of SSA emissions in marine models.

104 In the field, marine combined carbohydrates in aerosol particles (CCHO<sub>aer</sub>) have been  
105 predominantly measured at ship-based or coastal locations, which are in close proximity to  
106 local marine emission sources both horizontally and vertically (Leck et al., 2013; van Pinxteren  
107 et al., 2023; Zeppenfeld et al., 2021, 2023). In contrast, only a few studies have investigated  
108 CCHO<sub>aer</sub> (Karl et al., 2019; Yttri et al., 2024) at an elevated mountain site in a marine-influenced  
109 setting, aiming to assess atmospheric concentrations at higher altitudes. Vertically resolved  
110 field data comparing ground-level and elevated altitudes using mobile platforms for marine  
111 CCHO<sub>aer</sub> have, however, been lacking to date. Vertically resolved field data comparing ground-  
112 level and elevated altitudes using mobile platforms, however, have been unavailable for  
113 marine CCHO<sub>aer</sub> in the past. As a result, it remains unclear to what extent and under which  
114 conditions CCHO<sub>aer</sub> reach the upper marine boundary layer and the free troposphere. This is  
115 due to several methodological challenges, most fundamentally the absence of suitable high-  
116 resolution online detection techniques for CCHO<sub>aer</sub>, reflecting the inherent analytical difficulty  
117 of this compound class. As a consequence, current approaches rely on offline analyses, which  
118 are further constrained by low atmospheric concentrations that approach their detection  
119 limits. In addition, lightweight yet powerful high-flow pumps remain technically challenging to  
120 realize for mobile airborne platforms (e.g., drones or balloon-based systems), where payload  
121 and power constraints limit the collection of sufficient aerosol mass during short sampling  
122 periods. As a result, it remains unclear to what extent and under which conditions CCHO<sub>aer</sub>  
123 reach the upper marine boundary layer and the free troposphere, leaving high uncertainty  
124 about the broader relevance of these biomolecules for cloud formation and glaciation beyond  
125 controlled laboratory conditions, including low atmospheric concentrations pushing the  
126 instruments' detection capabilities for offline analyses to their limits, the lack of highly  
127 resolving online detection techniques for CCHO<sub>aer</sub>, and in particular the absence of lightweight  
128 yet powerful pumps with high flow rates. Additionally, the very short sampling times typically  
129 available on mobile airborne measurement platforms pose a further obstacle for measuring  
130 marine CCHO<sub>aer</sub> in aerosol particles across altitudes within the troposphere. This lack of  
131 vertical field data leaves high uncertainty about the broader relevance of these biomolecules  
132 in cloud formation and glaciation beyond a controlled laboratory setup.  
133 Previous airborne measurements around Svalbard (Hara et al., 2003; Simon et al., 2025) and  
134 the Canadian Arctic (Köllner et al., 2017) demonstrated that SSA particles, identified by Na<sup>+</sup>  
135 and Cl<sup>-</sup>, are present in higher altitudes of the lower troposphere, and, to a lesser extent, reach

hat formatiert: Nicht Hochgestellt/ Tiefgestellt

hat formatiert: Schriftart: 12 Pt.

hat formatiert: Schriftart: 12 Pt., Schriftfarbe:  
Automatisch

hat formatiert: Nicht Hervorheben

hat formatiert: Nicht Hervorheben

hat formatiert: Nicht Hervorheben

hat formatiert: Tiefgestellt, Nicht Hervorheben

hat formatiert: Nicht Hervorheben

hat formatiert: Nicht Hervorheben

hat formatiert: Hervorheben

136 the middle free troposphere (3–6 km a.s.l.). Some of these aerosol particles showed signs of  
137 atmospheric aging, such as the replacement of chloride with nitrate and sulfate in the SSA  
138 particles. While vertically resolved data exists for major inorganic SSA constituents, such  
139 extended information is lacking for marine CCHO<sub>aer</sub>.

140 Recent methodological advances now allow for a more detailed investigation of the transport  
141 mechanisms and atmospheric chemical fate of marine carbohydrates. In this study, we  
142 present atmospheric concentrations of these biomolecules alongside common inorganic SSA  
143 constituents. Measurements were conducted from ground level up to various altitudes within  
144 the boundary layer and lower free troposphere using a tethered helium balloon in Ny-Ålesund  
145 on Svalbard during autumn 2021 and spring 2022. For selected cases, we examined the  
146 influence of mixing state, meteorological conditions, and air mass history on the observed  
147 aerosol composition. Finally, this study addresses the potential atmospheric processing and  
148 transformation of marine carbohydrates, with a focus on their possible contribution to  
149 secondary aerosol formation and their implications for atmospheric chemistry and cloud-  
150 relevant processes.

## 2. Experimental Methods

This section summarizes the observational and modelling approaches used in this work. It covers the study area, field sampling, offline and online measurements, supporting datasets, model calculations, and statistical and visualization methods for data interpretation. An overview of all analytical and modelling methods relevant applied parameters and methods in this study is provided in Table 1.

Table 1. Overview of parameters, methods and sample/media types used in this study.

Category	Parameters	Method/Instrument	Sample/Medium
Major inorganic ions	Na <sup>+</sup> , K <sup>+</sup> , Mg <sup>2+</sup> , Ca <sup>2+</sup> , Cl <sup>-</sup> , SO <sub>4</sub> <sup>2-</sup> , oxalate	Ion chromatography	Bulk seawater, SML, aerosol particles (filter)
Free and combined carbohydrates	Fuc, Rha, Ara, Gal, Glc, Xyl, Man, Fru, GalN, GlcN, MurAc, GalAc, GlcAc	HPAEC-PAD	Bulk seawater, SML, aerosol particles (filter)
Sea surface temperature	SST	Digital Thermometer	Ocean surface
Aerosol number concentration	N <sub>150</sub> (150-2900 nm)	POPS (CAMP)	Atmospheric column
Meteorology	T, U, WD, RH, p, wind, $\theta$ , q	Standard meteorology package + thermodynamic equations	Atmosphere at ground (AWIPEV), atmospheric column
Cloud properties	Clouds and hydrometer types, IWP, LWP, IWV	Cloudnet + HATPRO	Atmospheric column
Biogeochemistry (model)	TChl-a, dissolved acidic polysaccharides	FESOM2.1-REcoM3	Ocean surface
Air mass origin	48-h back-trajectories	NOAA HYSPLIT	Several altitudes of atmosphere

### 2.1 Study area: Ny-Ålesund as an atmospheric observation site

Ny-Ålesund, located at 78.9°N at the Kongsfjorden in Svalbard (Norway), belongs to the world's northernmost permanently inhabited settlements with a year-round accessibility. It

162 serves as a key research site for studying Arctic climate change and Arctic amplification. Ny-  
163 Ålesund hosts long-term monitoring sites for aerosols and meteorology, such as the Zeppelin  
164 Observatory (Platt et al., 2022), Gruvebadet (Amore et al., 2022), and the AWIPEV Observatory  
165 (Maturilli et al., 2013, 2015). These, along with additional research stations operated by  
166 various international institutions, provide valuable data for both long-term atmospheric  
167 studies and short-term investigations like the present one.

168 However, Ny-Ålesund is not representative of the entire High Arctic. Its distinct topography,  
169 situated within a fjord and surrounded by high mountains up to 800 m, leads to complex  
170 atmospheric dynamics, including foehn-like effects (Shestakova et al., 2021). The local  
171 boundary layer is relatively shallow characterized by an average mixing layer height below  
172 700 m and a strong influence by orographic effects (Chang et al., 2017; Dekhtyareva et al.,  
173 2018; Gierens et al., 2020). While free-tropospheric winds are predominantly westerly,  
174 surface winds result from an interplay of land-sea breeze circulations, southeasterly  
175 channeled winds along the fjord axis, and katabatic flows from the Zeppelin mountain range,  
176 the Broeggerbreen glacier, or the Kongsvegen glacier (Esau and Repina, 2012; Gierens et al.,  
177 2020). Additionally, large wind shear has been observed to generate turbulence, leading to  
178 frequent neutral stratification (Gierens et al., 2020). Furthermore, boundary layer mixing can  
179 occur even when a positive gradient in potential temperature exists, suggesting a more stable  
180 stratification. During the present field campaign, we observed that near-surface winds often  
181 shift unpredictably, changing direction without a clear pattern, making airflow dynamics  
182 challenging to interpret.

183 From an oceanographic perspective, Svalbard is similarly exceptional. The region is influenced  
184 by the cold Arctic waters of the Spitsbergen Polar Current and the warm waters of the West  
185 Spitsbergen Current (Feltracco et al., 2021). Kongsfjorden, located on the western coast of  
186 Spitsbergen, lies at the interface of High Arctic and Atlantic influences, making it a dynamic  
187 and variable environment (Bischof et al., 2019).

188 Therefore, findings from Ny-Ålesund may not be fully transferable to atmospheric processes  
189 over sea ice or the open ocean in the High Arctic. However, in general, the representativeness  
190 of any single Arctic site is highly questionable, as Freud et al., (2017) found significant  
191 heterogeneity in aerosol particle size distribution across all Arctic sites in their study.

192 **2.2 Field sampling**

193 The field samples (aerosol particles, bulk seawater and SML) for this study were collected near  
194 Ny-Ålesund and from the adjacent Kongsfjorden during autumn 2021 and spring 2022.

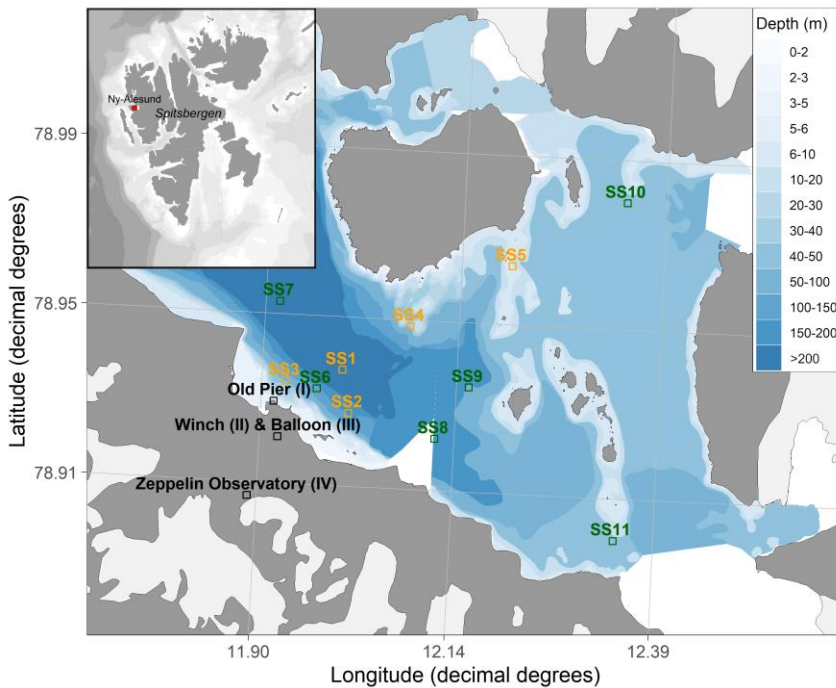


**Figure 1.** Map of the sampling locations. Aerosol particles were collected at: (I) the Old Pier, representing fresh SSA emissions; (II) the winch, representing ground measurements; (III) the tethered balloon at various altitudes; and (IV) the Zeppelin Observatory, serving as a reference for comparison. Bulk and SML samples were collected from different locations within Kongsfjorden. Orange squares (SS1-SS5) indicate autumn 2021 samples, while green squares (SS6-SS11) represent spring 2022 samples. Blue shading indicates water depth.

195

196 *a) Bulk seawater and SML sampling*

197 In total, 11 bulk surface seawater and 11 SML samples were taken from a small boat at various  
198 dates and locations across the Kongsfjorden (**Figure 1, Table S1**). Bulk water samples were  
199 obtained from a depth of 1 m using low-density polyethylene (LDPE) bottles secured to a  
200 telescopic rod. The corresponding SML samples were collected using the glass plate technique  
201 (Cunliffe and Wurl, 2014; van Pinxteren et al., 2012). A glass plate measuring  
202 50 cm × 20 cm × 0.5 cm, with an oval sampling area of 2000 cm<sup>2</sup>, was immersed vertically into

203 the surface of the fjord seawater and withdrawn at a steady rate of  $15 \text{ cm s}^{-1}$ . The SML film  
204 attached to the glass surface was drained into a precleaned wide-neck plastic bottle using a  
205 funnel and a framed Teflon wiper. Water samples were filtered through  $0.2 \mu\text{m}$  polycarbonate  
206 filters (Whatman® Nuclepore™, 47 mm diameter) to separate dissolved and particulate  
207 fractions. The filtrate, filters and field blanks were preserved at  $-20^\circ\text{C}$  until chemical analyses  
208 (inorganic ions, carbohydrates). Sea surface temperature (SST) was measured directly from  
209 the boat at a depth of approximately 10 cm using a digital thermometer.

210 *b) Aerosol particle sampling in the surroundings of Ny-Ålesund*

211 Total suspended aerosol particles (TSP) were captured on polycarbonate filters ( $0.8 \mu\text{m}$ ,  
212 Whatman® Nuclepore™, 47 mm diameter) at four locations (**Figure 1**): (I) Near the Old Pier  
213 next to Kongsfjorden (8 samples), representing fresh SSA emissions; (II) near the balloon winch  
214 close to the AWIPEV Observatory (17 samples), representing ground measurements; (III) at  
215 high altitudes at the tethered balloon (14 samples); and (IV) at the Zeppelin Observatory  
216 (1 sample), serving as a reference for comparison. **Table S2** provides details of individual  
217 aerosol particle samplings near the Old Pier (I), while **Table S3** presents the sampling times,  
218 locations and heights of all the individual high-altitude aerosol samples (III & IV), along with  
219 the corresponding simultaneous ground-level samples (II) taken near the winch.

220 For sampling aerosol particles at the Old Pier (4 m above sea level), a filter holder with a  
221 polycarbonate filter attached to a pump was used. Sampling lasted between 4 and 7 days.  
222 Flow rates, measured at the beginning and the ending of the sampling with a flowmeter,  
223 ranged from  $5$  to  $10 \text{ L min}^{-1}$ , with total air volumes between  $44$  and  $82 \text{ m}^3$ . The estimated  
224 diameter-dependent collection efficiency of this TSP sampling setup, assuming a  $90^\circ$   
225 aspiration angle, is shown in **Figure S1**. To reduce the risk of pump failure due to cold  
226 temperatures or snow, the pumps were housed in a Zarges box for protection.

227 High-altitude TSP samples were collected using the helium-filled tethered balloon BELUGA, as  
228 described in detail by Pilz et al. (2023). The balloon's altitude was controlled using an electric  
229 winch located near the AWIPEV Observatory, with ascent and descent rates from  $1$  to  $3 \text{ m s}^{-1}$ .  
230 The tethered balloon operated under various meteorological conditions, including both clear  
231 and cloudy skies. At a specified altitude, a HALFBAC (High-volume And Light-weight Filter  
232 sampler for BALloon-borne appliCation) (Grawe et al., 2023) collected aerosol particles 2-3 m  
233 below the balloon. The HALFBAC is a custom-designed, lightweight aerosol particle sampler

234 operating at a pump flow between 25 and 35 L min<sup>-1</sup>. It is capable of collecting sufficient  
235 aerosol mass on filters at high altitudes for subsequent offline chemical and microphysical  
236 analyses. Simultaneously, another HALFBAC collected ground-level aerosol particles near the  
237 electric winch (20 m above sea level). Additionally, one aerosol sample (Filter ID 62, sampling  
238 date: 10/05/2022) was collected at the Zeppelin Observatory, a permanent monitoring station  
239 located at 474 m a.s.l. on Zeppelinfjellet, using the HALFBAC. Synchronized aerosol particle  
240 sampling at the winch and the balloon typically lasted around two hours, as detailed in **Table**  
241 **S3**. The collection efficiency for TSP sampling using HALFBAC is discussed in the supplement  
242 (A1) and **Figure S1**.

243

### 244 **2.3 Chemical analyses from offline aerosol particle filters and seawater**

245 For the analysis of major cations, anions and marine carbohydrates in aerosol particles, the  
246 complete polycarbonate filters were extracted in 6-7 mL of ultrapure water  
247 (resistivity > 18.2 MΩ) for two hours followed by a filtration through a 0.45 μm syringe filter.  
248 Frozen seawater samples were ~~gently~~ thawed at 4°C in a refrigerator one day before analysis.

#### 249 *a) Major cations and anions*

250 Major inorganic ions, including sodium (Na<sup>+</sup>), potassium (K<sup>+</sup>), magnesium (Mg<sup>2+</sup>), calcium  
251 (Ca<sup>2+</sup>), chloride (Cl<sup>-</sup>), sulfate (SO<sub>4</sub><sup>2-</sup>), and oxalate, were quantified in 0.45 μm filtered aqueous  
252 aerosol extracts, bulk seawater and SML samples using ion chromatography (Dionex ICS-6000,  
253 Thermo Scientific) as described by Zeppenfeld et al. (2021). Cations were separated  
254 isocratically with a 36 mM methanesulfonic acid eluent on a Dionex IonPac CS16-4 μm column  
255 (2 mm × 250 mm), paired with a Dionex IonPac CG16-4 μm guard column (2 mm × 50 mm).  
256 For anion separation, a gradient from 4 to 40 mM KOH was applied on a Dionex IonPac AS18  
257 column (2 mm × 250 mm), along with a Dionex IonPac AG18 guard column (2 mm × 50 mm).  
258 The analytical uncertainty for each ion was below 5%. Aerosol extracts were measured  
259 undiluted, while bulk seawater and SML samples were analyzed at a 1:15,000 dilution.

260 *b) Dissolved free and combined carbohydrates*

261 Carbohydrates in seawater and aerosol particle extracts were measured according to the  
262 protocols outlined by Zeppenfeld et al. (2020, 2021), utilizing high-performance anion-  
263 exchange chromatography with pulsed amperometric detection (HPAEC-PAD). The system  
264 was equipped with a Dionex CarboPac PA20 analytical column (3 mm × 150 mm) and a Dionex  
265 CarboPac PA20 guard column (3 mm × 30 mm). The applied eluent gradient separated the  
266 following monosaccharide units: fucose (Fuc), rhamnose (Rha), arabinose (Ara), galactose  
267 (Gal), glucose (Glc), xylose (Xyl), mannose (Man), fructose (Fru), galactosamine (GalN),  
268 glucosamine (GlcN), muramic acid (MurAc), galacturonic acid (GalAc), and glucuronic acid  
269 (GlcAc). The analytical uncertainty for each monosaccharide was below 10%. ~~Dissolved free  
270 carbohydrates are measured without hydrolysis~~ FCHO represents the total of identifiable free  
271 ~~monosaccharides~~, whereas CCHO include ~~only~~ those monosaccharides released ~~through by~~  
272 acid hydrolysis (0.8 M HCl, 100°C, 20 h). For seawater samples, particulate combined  
273 carbohydrates (pCCHO, >0.2 µm) were measured from 0.2 µm polycarbonate filters, while  
274 dissolved combined carbohydrates (dCCHO, <0.2 µm) were measured from the filtrate after  
275 desalination via electrodialysis. Both fractions were later summed to represent the total  
276 CCHO. For the winch and balloon samples, the limited air volume and resulting low aerosol  
277 mass collected on the filters permitted quantification only of the major monosaccharides  
278 (typically Glc, Xyl, Gal, Ara), while minor monosaccharides remained largely below the  
279 instrumental detection limits. In contrast, samples from the Old Pier and surface seawater  
280 provided sufficient analyte mass to quantify the full suite of the CCHO monosaccharides.

281

282 **2.4 Vertical profiles from online measurements**

283 *a) Size-resolved aerosol particles number concentrations*

284 An optical particles size spectrometer (POPS, Handix), integrated into the Cubic Aerosol  
285 Measurement Platform (CAMP) as described by Pilz et al. (2022), provided the integrated total  
286 number concentrations ( $N_{150}$ ) for aerosol particles between 150 and 2900 nm at a temporal  
287 resolution of 1 second. On selected dates of HALFBAC sampling, CAMP was operated  
288 simultaneously 25 m below the balloon providing insight into the vertical profile of  $N_{150}$  during  
289 specific events. Vertical profiles are presented as rolling averages over 30 seconds.

290

291 *b) Meteorological observations and calculations*

292 Standard meteorological parameters, including altitude, ambient temperature (T), wind speed  
293 (U), wind direction (WD), air pressure (p), and relative humidity (RH), were measured for the  
294 elevated-altitude samples using a standard meteorology package positioned approximately  
295 20 m below the balloon (Pilz et al., 2023). The potential temperature ( $\theta$ ) within the  
296 atmospheric column - as a measure of the static stability of the unsaturated atmosphere - was  
297 calculated using Eq. I, where T is the ambient temperature (K), p is the atmospheric pressure  
298 (hPa),  $p_0$  is the reference pressure (1000 hPa), R is the specific gas constant ( $287 \text{ J kg}^{-1} \text{ K}^{-1}$ ) and  
299  $c_p$  is the specific heat capacity of dry air at constant pressure ( $1004 \text{ J kg}^{-1} \text{ K}^{-1}$ ).

300 
$$\theta = T \left( \frac{p_0}{p} \right)^{\frac{R}{c_p}} \quad (\text{Eq. I})$$

301 Specific humidity (q)–remaining constant during adiabatic ascent or descent as long as no  
302 phase changes occur–was calculated using Eq. II from Egerer et al. (2021), where  $R_d/R_v$  (the  
303 ratio of specific gas constants for dry air and water vapor) is approximately 0.622, and  $e_s(T)$   
304 represents the temperature-dependent saturation vapor pressure.

305 
$$q = \frac{R_d/R_v \cdot e_s(T) \cdot RH}{p - (1 - R_d/R_v) \cdot e_s(T) \cdot RH} \quad (\text{Eq. II})$$

306 Meteorological data measured 2 m above the ground (13 m above sea level) at the AWIPEV  
307 Atmospheric Observatory (Maturilli, 2020), represented the weather conditions during  
308 aerosol sampling at the winch.

## 309 2.5 Supporting observations and model calculations

310 Major inorganic ions measured at the Zeppelin Observatory with a 24-hour resolution using a  
311 statically installed aerosol sampler (Filter\_3pack) as part of the European Monitoring and  
312 Evaluation Programme (Tørseth et al., 2012) by the Norwegian Polar Institute (NPI) and the  
313 Norwegian Institute for Air Research (NILU) were obtained from the EBAS database for the  
314 study duration (Aas et al., 2022, 2023). The Filter\_3pack data were utilized in two ways:

- 315 1. **Comparing sampling techniques:** Data from the Filter\_3pack were compared with one  
316 HALFBAC aerosol particle sample collected directly at the Zeppelin Observatory (Filter  
317 ID 62, 10 May 2022) to evaluate potential artifacts arising from differences in sampling  
318 techniques and filter media. Despite variations in time resolution and methods,  
319 sodium, potassium, chloride, and sulfate concentrations showed strong agreement  
320 (detailed in the supplement A2 and **Figure S2**).
- 321 2. **Comparison with balloon data:** Sodium concentrations measured at the Zeppelin  
322 Observatory were directly compared with those obtained from the tethered balloon  
323 sampling.

324 Information on the occurrence of clouds and hydrometeor types at Ny-Ålesund were taken  
325 from the Cloudnet classification product (Illingworth et al., 2007; Nomokonova et al., 2019),  
326 which is based on a combination of ground-based cloud radar, ceilometer, and numerical  
327 weather prediction output. Vertically integrated ice water content (IWC), i.e. ice water path  
328 (IWP), has been calculated from the Cloudnet IWC product following Hogan et al. (2006).  
329 Vertically integrated cloud liquid water (liquid water path; LWP) and water vapor (IWV) were  
330 taken from zenith HATPRO microwave radiometer measurements (Nomokonova et al., 2019).

331 The 48-hour back-trajectories for the aerosol sampling periods were generated using the  
332 NOAA HYSPLIT model (Stein et al., 2015). Trajectories were calculated hourly based on GDAS1  
333 meteorological data (Global Data Assimilation System; 1° spatial resolution; 3-hour intervals)  
334 for various arrival heights: 50 m (ground level), 474 m (Zeppelin Observatory), and the specific  
335 balloon sampling altitudes. Sea ice concentration data were obtained from the NOAA-  
336 maintained ERDDAP server (Environmental Research Division's Data Access Program). The  
337 back-trajectories were used to assess the relative influence of distant sources, such as the  
338 marginal ice zone, versus local ice-free oceanic emissions on the aerosol chemical  
339 composition. Given the rather short atmospheric residence time of supermicron SSA particles

340 (Madry et al., 2011; Veron, 2015), which account for most of the SSA mass in TSP, and the  
341 increasing uncertainties associated with longer back-trajectory periods, we considered a 48-  
342 hour back-trajectory length appropriate for this analysis.

343 Ocean surface concentrations for total chlorophyll *a* (TChl-*a*) and dissolved acidic  
344 polysaccharides were obtained by a coupled setup of the ocean sea ice biogeochemistry  
345 model FESOM2.1-REcoM3 (Gürses et al., 2023), to which additional state equations have been  
346 added to simulate dissolved and particulate organic carbon following Engel et al. (2004) and  
347 Schartau et al. (2007). The simulation was set up following Gürses et al. (2023) and using the  
348 Arctic-specific tuning of Oziel et al. (2022). The modelled dissolved acidic polysaccharides were  
349 used as a proxy for dCCHO. Although they represent only a fraction of dCCHO, their  
350 concentrations were shown to be within the same order of magnitude as field observations  
351 (Zeising et al., 2026). Monthly model output was obtained on an irregular grid with  
352 approximately 4.5 km resolution in the Arctic Ocean. This configuration has already been  
353 applied successfully in Leon-Marcos et al. (2025).

354

## 355 **2.6 Statistics, data processing, visualization and text optimization**

356 Statistical analyses, calculations and visualization were conducted using OriginPro 2024,  
357 Microsoft Excel, IDL, python3 and R version 4.2.1 with the ncd4 (Pierce, 2023), openair  
358 (Carslaw and Ropkins, 2012), reshape2 (Wickham, 2007), scales (Wickham et al., 2023b),  
359 lubridate (Grolemund and Wickham, 2011), cmocean (Thyng et al., 2016), maps (Brownrigg,  
360 2023), mapdata (Brownrigg, 2013), rgdal (Bivand et al., 2022), raster (Hijmans, 2023),  
361 RColorBrewer (Neuwirth, 2022), sp (Bivand et al., 2013), dplyr (Wickham et al., 2023a), ggplot2  
362 (Wickham, 2016), and PlotSvalbard (Vihtakari, 2020) packages. Box-and-whisker plots  
363 illustrate the interquartile range (box), the median (horizontal line inside the box), the mean  
364 (open square), the minimum and maximum values (whiskers). Text and language were  
365 optimized using Open AI's ChatGPT-4 Turbo.

hat formatiert: Nicht Hervorheben

## 366 3. Results and Discussion

### 367 3.1 Chemical constituents in marine aerosol particles from their oceanic source 368 to elevated altitudes

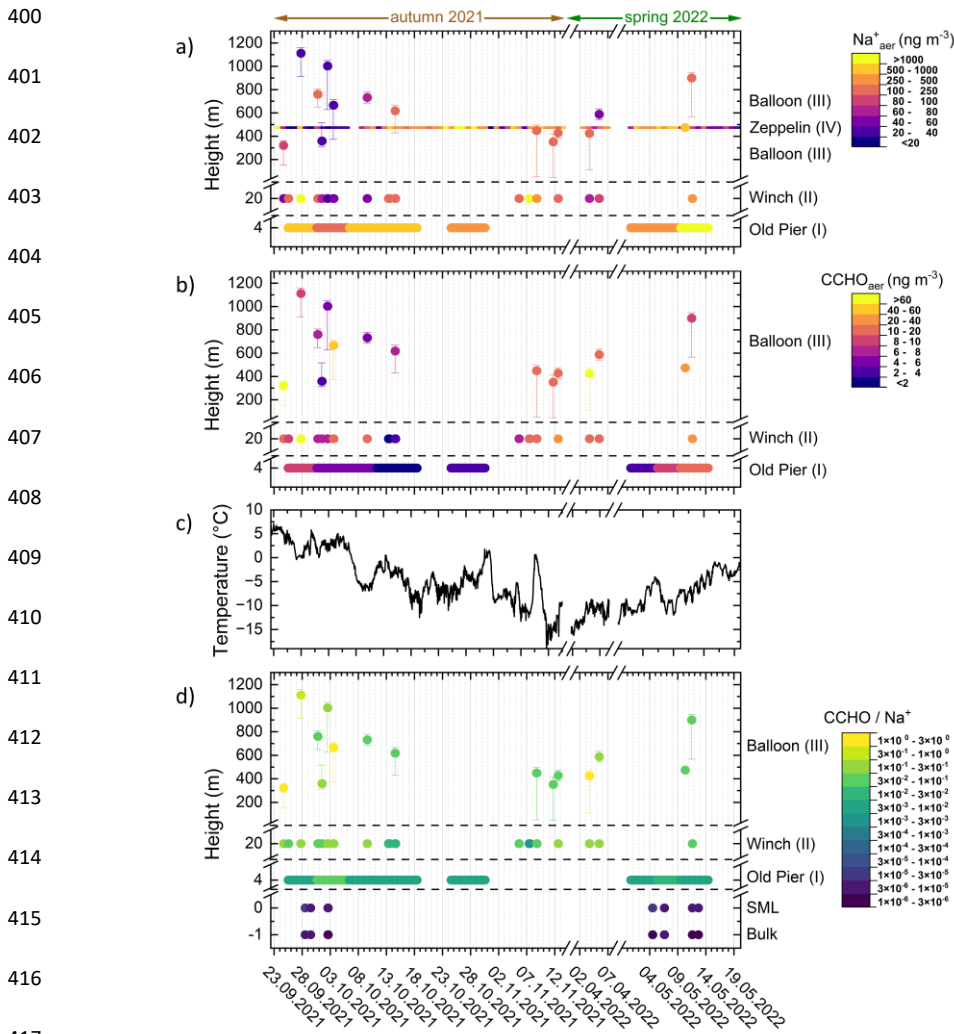
#### 369 *Sodium in aerosol particles ( $\text{Na}^+_{\text{aer}}$ )*

370 Sodium, a dominant and chemically stable component of SSA, is commonly used as a tracer  
371 for tracking ocean-derived emissions in atmospheric studies (Manders et al., 2010; van  
372 Pinxteren et al., 2017; White, 2008). In this study, consistently high  $\text{Na}^+_{\text{aer}}$  concentrations were  
373 observed on the TSP filters at the Old Pier next to Kongsfjorden in both autumn 2021 and  
374 spring 2022 (**Figure 2a**), ranging from 140 to 1470  $\text{ng m}^{-3}$  (median: 495  $\text{ng m}^{-3}$ ;  $n=8$ ). The area  
375 around Ny-Ålesund, especially the Old Pier, remained largely ice-free, indicating a negligible  
376 influence of local sea ice on SSA emissions.

377  $\text{Na}^+_{\text{aer}}$  at the winch site, located further inland but still at ground level (35–3710  $\text{ng m}^{-3}$ ;  
378 median: 155  $\text{ng m}^{-3}$ ;  $n=17$ ), and at the balloon (321–1112 m; 23–850  $\text{ng m}^{-3}$ ; median:  
379 124  $\text{ng m}^{-3}$ ;  $n=15$ ) was generally lower than at the Old Pier, though episodic high events  
380 occurred at all sites. This wide variability from low  $\text{ng m}^{-3}$  to a few  $\mu\text{g m}^{-3}$  agrees with  
381 observations from other marine environments and altitudes (Fomba et al., 2014; Li et al.,  
382 2024; Ooki et al., 2002; Theodosi et al., 2010; Triesch et al., 2021; Zeppenfeld et al., 2021,  
383 2023).

384 Since winch and balloon sampling were always synchronized, direct comparisons were  
385 possible (**Figure 3**). Several events showed nearly identical  $\text{Na}^+_{\text{aer}}$  concentrations (winch vs.  
386 balloon), e.g., 30 Sep: 191 -vs. 207  $\text{ng m}^{-3}$ ; 2 Oct: 35 -vs. 36  $\text{ng m}^{-3}$ ; 9 Oct: 59 -vs. 60  $\text{ng m}^{-3}$ ; 12  
387 Nov: 240 -vs. 223  $\text{ng m}^{-3}$ . In contrast, other periods exhibited strong vertical gradients with  
388 higher ground-level concentrations (e.g., 27 Sep: 1840 -vs. 23  $\text{ng m}^{-3}$ ; 5 Apr: 84 -vs. 54  $\text{ng m}^{-3}$ ;  
389 11 May: 496 -vs. 125  $\text{ng m}^{-3}$ ), while two cases showed higher values at the balloon (24 Sep:  
390 47 -vs. 99  $\text{ng m}^{-3}$ ; 3 Apr: 77 -vs. 194  $\text{ng m}^{-3}$ ). These variations are likely driven by atmospheric  
391 processes, including dry and wet deposition (Farmer et al., 2021), dilution during vertical and  
392 horizontal transport from the emission region (Wong et al., 2019), vertical mixing (Pilz et al.,  
393 2024) and differing air mass histories (Willis et al., 2018), which will be examined in detail for  
394 three selected cases later in this study.

395  $\text{Na}^+_{\text{aer}}$  at the Zeppelin Observatory largely agreed with the balloon measurements (56–213%  
 396 overall; 92–107% in five events; **Table S6**), despite differences in time resolution (24 h vs. 1–  
 397 2 h), sampling altitude, the horizontal distance between the sites, Svalbard’s complex  
 398 topography (Gierens et al., 2020; Shestakova et al., 2021), and the fact that meteorological  
 399 conditions and atmospheric mixing states have not yet been considered.



417 **Figure 2.** Time-resolved atmospheric concentrations of a)  $\text{Na}^+_{\text{aer}}$  and b)  $\text{CCHO}_{\text{aer}}$  in aerosol particles (TSP) collected in autumn  
 418 2021 and spring 2022 in Ny-Ålesund at several heights (m a.s.l.) from four sites: Old Pier, winch near the AWIPEV Observatory,  
 419 balloon and the Zeppelin Observatory. Dots represent the median height during the total sampling time and vertical error  
 bars represent maximum and minimum height of the sampler during the active sampling. The x-axis ticks represent the start  
 of each date at midnight. c) Air temperature (2 m above ground) measured at the AWIPEV Observatory. d)  $\text{CCHO}/\text{Na}^+$  ratios  
 within the bulk seawater, the SML and in the aerosol particles at several heights. In panel (a), the label “Balloon (III)” appears  
 twice because balloon sampling for sodium measurements occurred both below and above the fixed altitude of the Zeppelin  
 Observatory.

420 Overall,  $\text{Na}^+_{\text{aer}}$  was detectable up to 1100 m altitude, sometimes at levels comparable to those  
 421 near the emission source, indicating effective vertical mixing or transport to cloud-relevant  
 422 heights via advection. This vertical distribution is consistent with the aircraft-based SSA  
 423 measurements reported by Hara et al. (2003) and Köllner et al. (2017). Longer atmospheric  
 424 residence increases the exposure of SSA particles to processing, which can alter their impact  
 425 on cloud formation. While  $\text{Na}^+_{\text{aer}}$  is considered chemically stable, co-emitted OM including  
 426 carbohydrates may undergo physical, chemical and microbial changes (Zeppenfeld et al.,  
 427 2021, 2023). This aspect will be explored further in section 3.3.

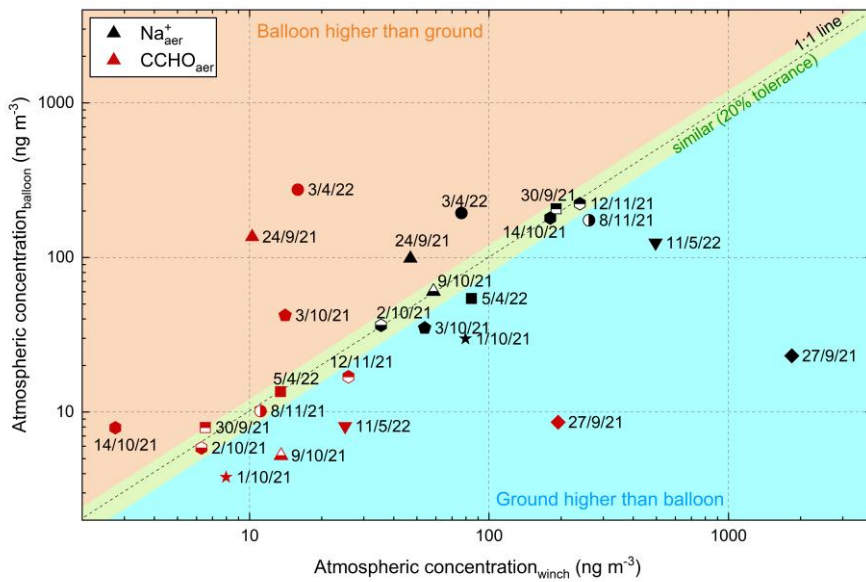


**Figure 3.** Scatter plot showing  $\text{Na}^+_{\text{aer}}$  (black symbols) and  $\text{CCHO}_{\text{aer}}$  (red symbols) concentrations in TSP measured at the winch, and balloon levels. Marker shapes and fill styles serve as identifiers linking corresponding  $\text{Na}^+_{\text{aer}}$  and  $\text{CCHO}_{\text{aer}}$  values from the same sample. Data points are categorized to indicate whether values were similar, higher at the balloon, or higher at the ground.

428

429

430

431

432 **Combined carbohydrates in fresh SSA and surface their-oceanic-origin-seawater**

433 Similar to sodium, CCHO<sub>aer</sub> were detected at all sites and altitudes (**Figure 2b**). At the Old Pier,  
434 CCHO<sub>aer</sub> concentrations ranged from 1.6 to 10.0 ng m<sup>-3</sup> (median: 5.0 ng m<sup>-3</sup>; n=8), showing a  
435 seasonal pattern with the highest values at the beginning (end of September 2021) and end  
436 (mid of May 2022) of the study period, and lower values in October 2021, coinciding with low  
437 air temperatures (**Figure 2c**). -No samples were collected between November and April, so  
438 winter trends remain unknown.

439 ~~The seasonal variation of CCHO<sub>aer</sub> at the Old Pier may be linked to the seasonal dynamics of~~  
440 ~~marine CCHO in the surface water of Kongsfjorden, the only local emission source of SSA.~~  
441 ~~These dynamics are likely driven by seasonal shifts in primary production and phytoplankton~~  
442 ~~composition (Assmy et al., 2023; Mayot et al., 2018; van de Poll et al., 2021).~~

443 A seasonal trend ~~Similar seasonality~~ was also observed for ~~selected monosaccharides among~~  
444 ~~dissolved combined carbohydrates (dCCHO)~~ in Kongsfjorden seawater. Concentrations  
445 peaked in late September/early October and were substantially lower in early to mid-May,  
446 averaging only about 50% of the autumn values (Figure 4). Most monosaccharides in bulk  
447 dCCHO showed a strong co-variation with SST ( $R^2 = 0.79-0.93$ ;  $n = 11$ ). This relationship was  
448 weaker for xylose ( $R^2_{Xyl-SST} = 0.62$ ) and glucose ( $R^2_{Glc-SST} = 0.53$ ) in bulk dCCHO, and generally  
449 more moderate in the SML for most monosaccharides. In particular, fucose, galactosamine,  
450 and rhamnose in bulk water dCCHO exhibited a distinct pattern, closely following SST. Their  
451 concentrations peaked in late September/early October, while being much lower (44-67%) in  
452 early to mid-May (**Figure 4**). This pattern was weaker for glucose in bulk dCCHO and even less  
453 pronounced in the SML for most monosaccharides (**Figure 4**).

454 In contrast, ~~particulate combined carbohydrates (pCCHO)~~ as a whole showed no clear  
455 seasonal trend in seawater (**Figure S3**). However, a few monosaccharides within bulk water  
456 pCCHO, in particular fucose, glucosamine, and galactosamine, displayed a moderate  
457 correlation with SST ( $R^2_{Fuc-SST} = 0.73$ ;  $R^2_{GalN-SST} = 0.39$ ;  $R^2_{GlcN-SST} = 0.69$ ;  $n=11$ ). -While dCCHO in  
458 bulk water exhibited relatively low spatial and intra-seasonal variability, pCCHO and SML  
459 samples were considerably more variable, even among samples from the same season (**Figure**  
460 **S4**). This likely reflects the rapid dynamics of pCCHO's in relation to phytoplankton blooms  
461 (Becker et al., 2020; Engel et al., 2012; Fabiano et al., 1993), as well as the formation of

hat formatiert: Hochgestellt

hat formatiert: Tiefgestellt

hat formatiert: Tiefgestellt

hat formatiert: Hochgestellt

hat formatiert: Tiefgestellt

hat formatiert: Tiefgestellt

hat formatiert: Tiefgestellt

462 transparent exopolymer particles (TEP) formation from dCCHO in turbulent waters, and  
463 vertical transport of pCCHO ~~through~~ via sedimentation (e.g., as marine snow) or its  
464 accumulation in the SML depending on buoyancy (Burns et al., 2019; Engel, 2004; Robinson et  
465 al., 2019<sup>ba, ba</sup>; Wurl and Holmes, 2008). The SML, in particular, may be more sensitive to  
466 these dynamics than the bulk water, potentially explaining its greater fluctuations.

hat formatiert: Schriftart: 12 Pt.

467

468

469

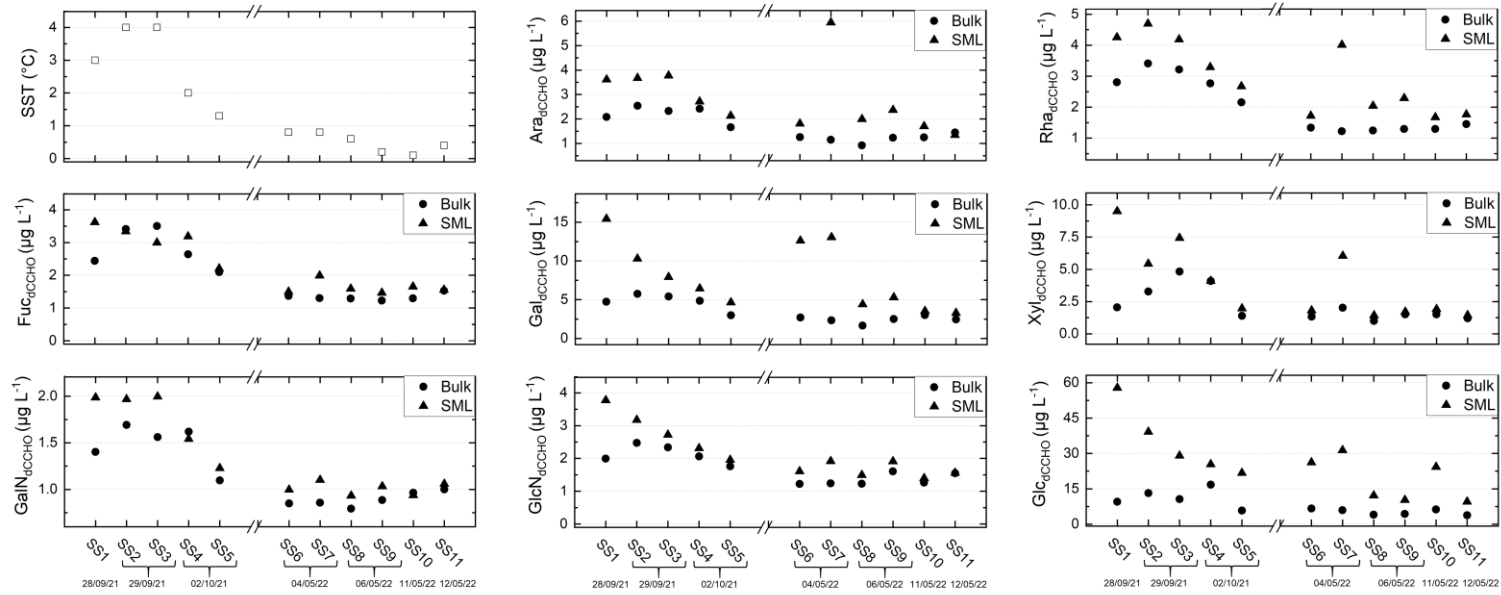
470

471

472

473

474



475

**Figure 4.** Concentration of measured monosaccharide units in dCCHO from bulk and SML samples collected in Kongsfjorden during autumn 2021 and spring 2022, along with SST measurements taken from bulk samples at the time of sampling.

476

477 ~~On the other hand~~By comparison, dCCHO in bulk water, like dissolved organic carbon (Hansell,  
478 2013; Keene et al., 2017), is likely dominated by recalcitrant and semi-recalcitrant compounds,  
479 while the labile fraction is rapidly consumed by heterotrophic bacteria (Goldberg et al., 2011).  
480 Notably, combined glucose showed high variability in both dCCHO and pCCHO, likely due to  
481 being the main constituent of abundant storage macromolecules such as laminarin (Becker et  
482 al., 2020), whose production and turnover may be enhanced during periods of photosynthetic  
483 overflow (Barthelmeß et al., 2025), as well as its relatively rapid microbial utilization (Kharbush  
484 et al., 2020).

485 The seasonal variation of CCHO<sub>aer</sub> at the Old Pier may be linked to the seasonal dynamics of  
486 marine CCHO in the surface waters of Kongsfjorden, the only local emission source of SSA.  
487 These dynamics are likely driven by seasonal shifts in primary production and phytoplankton  
488 composition (Assmy et al., 2023; Mayot et al., 2018, van de Poll et al., 2021).

489  
490 Overall, CCHO<sub>aer</sub> and selected seawater dCCHO monosaccharides showed a broadly consistent  
491 seasonal tendency, with elevated values in late summer/early autumn. However, the spring  
492 conditions (May) deviate from this pattern, with CCHO<sub>aer</sub> showing a secondary maximum that  
493 is not reflected in seawater dCCHO, where concentrations remain substantially lower. This  
494 indicates that the seasonal coupling between (bulk) seawater CCHO and CCHO<sub>aer</sub> is strongest  
495 in late summer/early autumn, while additional processes such as SML enrichment or  
496 atmospheric processing may also contribute to the spring aerosol signal.

497 In conclusion, the seasonal variation of CCHO<sub>aer</sub> measured at the Old Pier is partly consistent  
498 with marine carbohydrates in Kongsfjorden seawater, suggesting that surface CCHO is an  
499 important but not exclusive source of freshly emitted CCHO<sub>aer</sub>.

500 ~~In conclusion, the seasonal variation of CCHO<sub>aer</sub> aligns with certain marine carbohydrates in~~  
501 ~~Kongsfjorden, suggesting surface dCCHO as the main source of freshly emitted CCHO<sub>aer</sub>.~~

## 502 **CCHO<sub>aer</sub> at the winch and higher altitudes**

503 CCHO<sub>aer</sub> at the winch site (1.9–194 ng m<sup>-3</sup>; median: 10.6 ng m<sup>-3</sup>; n=17) and at the balloon (3.8–  
504 274 ng m<sup>-3</sup>; median: 10.2 ng m<sup>-3</sup>; n=15), showed broader ranges and significantly higher

hat formatiert: Englisch (Vereinigtes Königreich)

hat formatiert: Englisch (Vereinigtes Königreich),  
Tiefgestellt

hat formatiert: Englisch (Vereinigtes Königreich)

hat formatiert: Englisch (Vereinigtes Königreich)

hat formatiert: Englisch (Vereinigtes Königreich)

hat formatiert: Englisch (Vereinigtes Königreich)

hat formatiert: Englisch (Vereinigtes Königreich)

hat formatiert: Englisch (Vereinigtes Königreich),  
Tiefgestellt

hat formatiert: Englisch (Vereinigtes Königreich)

hat formatiert: Englisch (Vereinigtes Königreich)

hat formatiert: Englisch (Vereinigtes Königreich),  
Tiefgestellt

hat formatiert: Englisch (Vereinigtes Königreich)

hat formatiert: Englisch (Vereinigtes Königreich),  
Tiefgestellt

hat formatiert: Englisch (Vereinigtes Königreich)

505 median and maximum values than at the Old Pier (**Figure 2b**), suggesting sources beyond  
506 primary sea-air transfer. Unlike the Old Pier, no clear seasonal pattern or altitude dependence  
507 was observed, likely due to the winch site's inland location, making it more sensitive to wind  
508 direction and changing weather. Also, the higher temporal resolution of the samples likely  
509 captured short-term fluctuations rather than integrated seasonal trends. In addition,  
510 atmospheric processing during transport and the lack of true winter samples may have further  
511 obscured any clear seasonal signal.

512 Similar to sodium, some events (**Figure 3**) showed comparable CCHO<sub>aer</sub> at the winch and  
513 balloon (e.g., 30 Sep: 6.5 vs. 8.0 ng m<sup>-3</sup>; 2 Oct: 6.3 vs. 5.8 ng m<sup>-3</sup>; 8 Nov: 11.1 vs. 10.2 ng m<sup>-3</sup>),  
514 while on other dates, concentrations were markedly lower at higher altitudes (e.g., 27 Sep:  
515 194 vs. 8.6 ng m<sup>-3</sup>; 11 May: 25 vs. 8.1 ng m<sup>-3</sup>), or conversely, higher aloft (e.g., 24 Sep: 10.2 vs.  
516 136 ng m<sup>-3</sup>; 3 Apr: 15.9 vs. 275 ng m<sup>-3</sup>). In most cases, CCHO<sub>aer</sub> covaried with sodium except on  
517 03 Oct, when Na<sup>+</sup><sub>aer</sub> was slightly higher at the ground (54 vs. 35 ng m<sup>-3</sup>), whereas CCHO<sub>aer</sub> was  
518 higher at the balloon (42 ng m<sup>-3</sup>) than at the winch (14 ng m<sup>-3</sup>).

519 To investigate oceanic emission and the atmospheric fate of marine CCHO, CCHO/Na<sup>+</sup> ratios  
520 were calculated for all aerosol, bulk seawater and SML samples, representing the primary  
521 sources of the SSA particle constituents studied here (**Figure 2d**). Bulk seawater showed the  
522 lowest ratios ( $2.0 \times 10^{-6}$ – $6.0 \times 10^{-6}$ ) with minimal variability, while the SML had slightly higher  
523 ratios ( $3.3 \times 10^{-6}$ – $2.5 \times 10^{-5}$ ) due to CCHO enrichment. Specifically, the enrichment factors  
524 (EF<sub>SML</sub>) ranged 1.3–4.1 for dCCHO and 0.9–6.8 for pCCHO (**Figure S4**), which aligns well with  
525 previous studies (Engel and Galgani, 2016; Gao et al., 2012; Zäncker et al., 2021; Zeppenfeld  
526 et al., 2021, 2023).

527 At the Old Pier, where fresh SSA was sampled, the ratios were significantly higher ( $6.2 \times 10^{-3}$   
528 –  $3.3 \times 10^{-2}$ ) indicating the chemo-selective sea-air transfer that enriches surface-active  
529 organics relative to sodium in aerosol particles (Hasenecz et al., 2020, 2019; Jayarathne et al.,  
530 2016; Schill et al., 2018; Zeppenfeld et al., 2021, 2023). The enrichment effect is typically more  
531 pronounced in submicron particles, which have a higher relative contribution of organics than  
532 inorganic ions (Quinn et al., 2015). In contrast, supermicron particles are predominantly  
533 composed of sea salts, although organic substances are still notably enriched compared to the  
534 surface seawater. As total suspended particles were measured here, and most SSA mass

535 resides in the supermicron range (Facchini et al., 2008; O'Dowd et al., 1997), our results  
536 primarily reflect supermicron aerosol composition.

537 At the winch sampling station, located at ground level but further inland, the CCHO/Na<sup>+</sup> ratios  
538 in TSP ranged from  $2.9 \times 10^{-3}$  to  $2.6 \times 10^{-1}$ , similar or slightly higher than at the Old Pier. In  
539 contrast, balloon samples from elevated altitudes showed higher ratios ( $3.9 \times 10^{-2}$ – $1.4 \times 10^0$ ),  
540 likely due to depletion of salt-rich supermicron particles during dry and wet deposition (Croft  
541 et al., 2009; Hoppel et al., 2002; O'Dowd and de Leeuw, 2007), increasing the relative  
542 contribution of OM-dominated submicron particles. Furthermore, the increasing absolute  
543 concentration of CCHO at higher altitudes (**Figure 2b**) suggests an atmospheric formation  
544 process contributing to the elevated CCHO/Na<sup>+</sup> ratios, potentially linked to microbial activity  
545 in the atmosphere (see section 3.3). However, because only the major monosaccharides  
546 (typically Glc, Xyl, Gal, Ara) could be quantified reliably in the winch and balloon samples,  
547 relative CCHO compositions were not assessed across the entire vertical sample set.  
548 Therefore, they were not used to further substantiate this conclusion, as it has been done in  
549 Zeppenfeld et al. (2021, 2023).

550 The CCHO/Na<sup>+</sup> ratios observed at the Old Pier and the Winch closely align with ship-based  
551 measurements ~~in the High Arctic during from~~ the PASCAL cruise ~~( $2 \times 10^{-3}$  to  $2 \times 10^{-1}$  for PM<sub>10</sub>~~  
552 ~~from summed Berner impactor stages) (conducted in May–July 2017) in the Fram Strait,~~  
553 ~~Barents Sea, and central Arctic Ocean (Macke and Flores, 2018; Wendisch et al., 2018), where~~  
554 ~~values ranged from  $2 \times 10^{-3}$  to  $2 \times 10^{-1}$  (in PM<sub>10</sub> based on summed Berner impactor stages~~  
555 ~~(Zeppenfeld et al., 2023)).~~ In contrast, the very high CCHO/Na<sup>+</sup> values ( $>1 \times 10^0$ ) observed at  
556 some elevated altitudes in this study were reported only occasionally for submicron particles  
557 (0.14–0.42 μm) during PASCAL. This may support the idea that supermicron particle  
558 deposition caused the shift in balloon sample ratios, though microbial contributions in the  
559 atmosphere are also possible. Moreover, these ratios far exceed those from the Southern  
560 Ocean near the western Antarctic Peninsula ( $8 \times 10^{-4}$  to  $7 \times 10^{-3}$ ) (Zeppenfeld et al., 2021),  
561 likely due to differences in surface seawater productivity.

562 Overall, it can be concluded that both Na<sup>+</sup><sub>aer</sub> and CCHO<sub>aer</sub> are transported from the marine  
563 emission source to elevated heights within the lower troposphere. In the following section,  
564 we discuss the role of meteorological conditions and atmospheric mixing in linking ground-  
565 based and balloon-based samples.~~However, with longer atmospheric residence times, the~~

hat formatiert: Tiefgestellt

566 ~~chemical composition of aerosol particles appears increasingly altered in certain samples. As~~  
567 ~~a key factor influencing these observations, the role of meteorological conditions and~~  
568 ~~atmospheric mixing in linking ground and balloon samples will be discussed in the next section.~~

569 **3.2 Impact of meteorological conditions on SSA particle constituents in higher**  
 570 **altitudes**

571 To examine how meteorological conditions and atmospheric mixing influenced  $\text{Na}^+_{\text{aer}}$  and  
 572  $\text{CCHO}_{\text{aer}}$  at elevated-high altitudes, three distinct cases with ~~distinct, unvarying~~ constant  
 573 weather conditions were selected (**Figure 5**). These conditions allow for a detailed  
 574 interpretation of the observed chemical values.

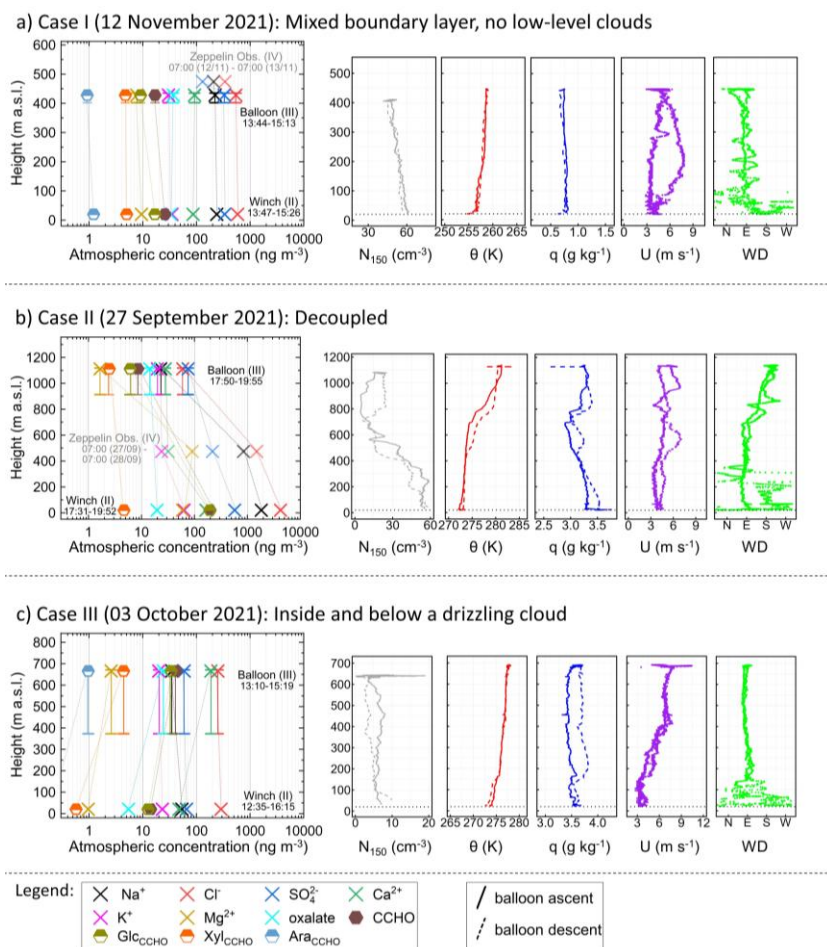


**Figure 5.** Vertical profiles of three atmospheric cases showing mass concentrations of chemical constituents (inorganic ions, oxalate, total  $\text{CCHO}_{\text{aer}}$ , and major monosaccharides within  $\text{CCHO}_{\text{aer}}$ ) in aerosol particles, measured on the ground (winch) and aloft (balloon) using offline filters. Vertical error bars indicate the range between minimal and maximal heights during active sampling at the balloon, while the symbols denote the median sampling heights. Data from the Zeppelin Observatory are also included when available and above detection limits, albeit with a 24-hour resolution. Dotted lines are included to aid in reading the vertical distribution of individual chemical substances. These profiles are complemented by aerosol particle number concentrations of particles bigger than 150 nm ( $N_{150}$ ), potential temperature ( $\theta$ ), specific humidity ( $q$ ), wind speed ( $U$ ), and wind direction ( $WD$ ) measured during the ascents (solid lines) and descents (dashed lines) of the balloon.

575 To assess atmospheric stability and layering in these cases, vertical profiles of potential  
 576 temperature were utilized. To further confirm aerosol mixing conditions, additional  
 577 meteorological parameters (specific humidity, wind speed and direction), vertical aerosol  
 578 particle number concentrations of particles larger than 150 nm ( $N_{150}$ ) (**Figure 5**), cloud  
 579 conditions (**Figure S5**) and back-trajectory analyses (**Figure 6**) were considered. The selected  
 580 cases include (a) a cloud-free mixed boundary layer (12 Nov 2021), (b) a free troposphere  
 581 decoupled from the ground (27 Sep 2021), and (c) a boundary layer capped by precipitating  
 582 clouds (03 Oct 2021).

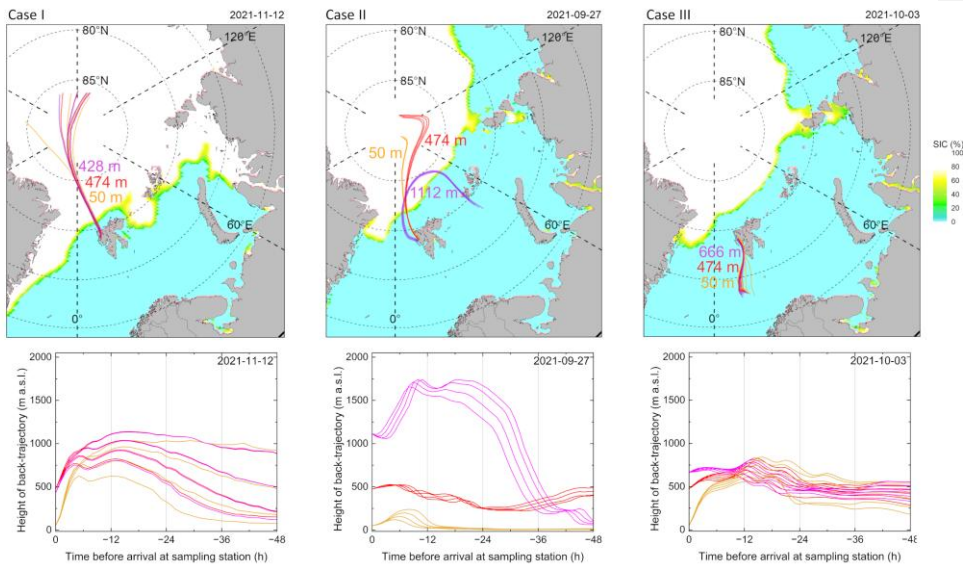


**Figure 6.** 48-hour back-trajectories calculated on an hourly basis for three arrival heights: orange (50 m, ground-level air masses), red (474 m, height of the Zeppelin Observatory), and purple (variable arrival height, high-altitude air masses sampled at sampled at tethered balloon). These are accompanied by daily sea ice concentration (SIC) maps (top) and height profiles (bottom) for three selected aerosol particle sampling cases.

583 **Case I: Mixed boundary layer & no low-level clouds**

584 On 12 November 2021, during the polar night, two HALFBACs were operated simultaneously  
 585 at the ground and the balloon (median altitude of 428 m) for approximately 90 min. Ground-  
 586 level conditions were  $-16.7^{\circ}\text{C}$ , 69% RH, and  $1.5\text{ m s}^{-1}$  wind mainly from the southwest. At the  
 587 balloon, sampling occurred at a similar temperature ( $-17.5^{\circ}\text{C}$ ) and RH (72%), but higher wind  
 588 speeds ( $4.3\text{ m s}^{-1}$ ) from the northeast to southeast. With  $\text{IWV} < 3\text{ kg m}^{-2}$ , the atmosphere was  
 589 very dry (**Figure S5a**), and only a thin mixed-phase cloud layer at 4.5–5 km altitude was

590 present, with negligible LWP and IWP (**Figure S5a**), unlikely to affect aerosol chemistry within  
591 the boundary layer.

592 During the balloon's ascent, potential temperature increased from 255 K to 258 K, with the  
593 strongest gradient near the ground. Using the wind speed profile and the Richardson number  
594 approach (Akansu et al., 2023), a very shallow surface mixing layer of ~12 m was estimated,  
595 likely caused by recent surface cooling. Although this surface inversion and the slightly stable  
596 to near-neutral stratification above would limit instantaneous vertical mixing, surface mixing  
597 layer height reflects only momentary conditions, whereas aerosol and humidity profiles  
598 integrate mixing over longer timescales. The coupling state at the time of measurement is  
599 therefore not a reliable indicator of the effective boundary-layer mixing state. Furthermore,  
600 as noted in Section 2.1, Ny-Ålesund's complex orography can induce localized turbulent mixing  
601 even under stable stratification. In addition, a low-level jet observed during descent, with wind  
602 speeds at least 2 m s<sup>-1</sup> higher than above and below, provided a significant additional source  
603 of turbulence and vertical mixing within the boundary layer (Egerer et al., 2023).

604 At the ground, N<sub>150</sub> was around 60 cm<sup>-3</sup>, and gradually decreased to 45 cm<sup>-3</sup> at the balloon's  
605 sampling height, indicating a fairly uniform aerosol distribution dominated by primary  
606 emissions. Combined with nearly constant specific humidity (~0.7–0.8 g kg<sup>-1</sup>), a slight wind  
607 speed increase with altitude, the low-level jet during descent, and consistent wind direction  
608 (**Figure 4a**), these suggest a largely well-mixed boundary layer. HALFBAC samples from ground  
609 and balloon showed similar concentrations of inorganic ions (Na<sup>+</sup><sub>aer</sub>: 240 & 223, Cl<sup>-</sup><sub>aer</sub>: 586 &  
610 543, SO<sup>2-</sup><sub>4 aer</sub>: 336 & 330, Ca<sup>2+</sup><sub>aer</sub>: 87 & 92, Mg<sup>2+</sup><sub>aer</sub>: 9.5 & 7.8, K<sup>+</sup><sub>aer</sub>: 34 & 30 ng m<sup>-3</sup>), oxalate<sub>aer</sub>  
611 (34 & 37 ng m<sup>-3</sup>), and major CCHO-bound monosaccharides (Glc<sub>CCHO,aer</sub>: 17 & 9.1, Xyl<sub>CCHO,aer</sub>:  
612 5.0 & 4.7, Ara<sub>CCHO,aer</sub>: 1.2 & 0.9 ng m<sup>-3</sup>), supporting a well-mixed layer. Despite diverse sources  
613 (SSA, dust, anthropogenic, secondary), vertical aerosol composition remained uniform.  
614 Zeppelin Observatory 24 h measurements of Na<sup>+</sup><sub>aer</sub>, Cl<sup>-</sup><sub>aer</sub>, and SO<sup>2-</sup><sub>4</sub> showed slightly lower  
615 concentrations but agreed with balloon results.

616 Back-trajectory analysis revealed that air masses at ground level, the balloon, and Zeppelin  
617 Observatory (**Figure 6, Case I**) followed the same path during the 48 hours before sampling.  
618 Originating from the Arctic pack ice, they crossed the marginal ice zone with a short residence  
619 time before passing over the ice-free ocean and Kongsfjorden, where most SSA compounds  
620 were likely taken up. The back-trajectory heights indicate a vertical connection between the

621 three air masses, confirming a similar transport history, influenced by the same emission  
622 sources.

623 This case demonstrates that major SSA constituents ( $\text{Na}_{\text{aer}}^+$ ,  $\text{Cl}_{\text{aer}}^-$ , and  $\text{CCHO}_{\text{aer}}$ ) can mix  
624 effectively within the boundary layer, reaching altitudes relevant to cloud formation with  
625 concentrations nearly identical to ground level, and that such a mixing state can persist during  
626 temporarily decoupled conditions, provided there is no additional aerosol particle source at  
627 the ground or aloft.

#### 628 ***Case II: Free troposphere decoupled from the ground***

629 On 27 September 2021, balloon measurements were conducted at a median altitude of  
630 1112 m, above both the Zeppelin Observatory and the altitude range of Case I, i.e. in the free  
631 troposphere above the boundary layer. A strong increase of the potential temperature  
632 between 700 m ( $\theta \approx 274$  K) and 900 m ( $\theta \approx 280$  K) indicates a pronounced inversion (**Figure 5b**).  
633  $\text{N}_{150}$  peaked near the ground, remained stable in the lowest 200 m, decreased up to  $\sim 700$  m,  
634 and slightly increased toward 1112 m, suggesting sources other than the ground. Specific  
635 humidity varied strongly (2.6–4 g kg<sup>-1</sup>), confirming a decoupled atmospheric layer.

636 During ground sampling, mean conditions were 3 °C, 89 % RH, and 0.7 m s<sup>-1</sup> wind from the  
637 southwest (**Table S5**). At balloon altitude, air was colder (-1.9 °C), slightly drier (87 % RH), and  
638 much windier (5.5 m s<sup>-1</sup>), primarily from the south and southwest (**Table S4**). IWV increased  
639 from 13 to  $\sim 15$  kg m<sup>-2</sup> during sampling (**Figure S5b**). A dense warm-front cloud layer (2–8 km)  
640 with mainly cloud ice (IWP up to 1.4 kg m<sup>-2</sup>) was present (**Figure S5b**). Precipitation reached  
641 the balloon as snowfall only in the last 15–30 min of sampling.

642 On this date, we observed a strong vertical gradient in both  $\text{Na}_{\text{aer}}^+$  and  $\text{CCHO}_{\text{aer}}$  concentrations  
643 (**Figure 5b**), starting from the winch ( $\text{Na}_{\text{aer}}^+$ : 1840 ng m<sup>-3</sup>,  $\text{CCHO}_{\text{aer}}$ : 199 ng m<sup>-3</sup>), decreasing at  
644 the Zeppelin Observatory ( $\text{Na}_{\text{aer}}^+$ : 850 ng m<sup>-3</sup>), and dropping sharply at the balloon's altitude  
645 ( $\text{Na}_{\text{aer}}^+$ : 23 ng m<sup>-3</sup>,  $\text{CCHO}_{\text{aer}}$ : 8.6 ng m<sup>-3</sup>). Similar declines occurred for  $\text{SO}_4^{2-}_{\text{aer}}$  (580; 220;  
646 76 ng m<sup>-3</sup>),  $\text{Cl}_{\text{aer}}^-$  (4230; 1500; 60 ng m<sup>-3</sup>), and  $\text{Ca}_{\text{aer}}^{2+}$  (165; 32; 28 ng m<sup>-3</sup>). This pronounced  
647 decrease with altitude indicates separation between ground-level and elevated air masses,  
648 making fresh local SSA from Kongsfjorden or the west coast of Svalbard an unlikely source for  
649 the substances detected at 1112 m.

650 This assumption is supported by back-trajectory analysis (**Figure 6b**): air masses at 50 m and  
651 474 m arrival height originated from Arctic pack ice and crossed the ice-free Fram Strait,  
652 whereas the 1112 m air mass followed a different path over the Barents Sea near Franz Josef  
653 Land. After contact with the marine boundary layer and possibly the sea surface about 48 h  
654 before sampling, it remained mainly between 1000 and 1800 m. This indicates that the SSA  
655 observed at 1112 m in Ny-Ålesund likely originated from this distant source region.

656 In summary, Case II demonstrates that major SSA constituents ( $\text{Na}_{\text{aer}}^+$ ,  $\text{Ca}_{\text{aer}}^{2+}$ ,  $\text{Cl}_{\text{aer}}^-$ ,  $\text{SO}_4^{2-}$   
657 and  $\text{CCHO}_{\text{aer}}$ ) can be present in the free troposphere and likely originate from a distant source.  
658 However, they appear at ~~different-lower~~ concentrations above the ~~temperature~~-inversion  
659 than ~~in~~ the ~~mixed~~ boundary layer below, where concentrations, ~~as~~like in Case I, are ~~more~~  
660 similar ~~to those at the ground~~.

#### 661 ***Case III: Inside and below a drizzling cloud***

662 On 03 October 2021, the ground temperature was 3°C with a high relative humidity of 89%.  
663 Winds were light, shifting between east, south, and west at 0.7 m s<sup>-1</sup> during sampling. At the  
664 balloon's altitude of 666 m, the average temperature was -1.3°C, the relative humidity 96%  
665 and the wind speed 6.8 m s<sup>-1</sup> from the east and northeast. The day was overcast, with  
666 continuous drizzle from a 2 km deep mixed-phase cloud layer with LWP values of up to  
667 300 g m<sup>-2</sup> and IWV of around 13 to 14 kg m<sup>-2</sup>. The balloon's altitude was close to the melting  
668 layer.

669 During the balloon's ascent and descent to 666 m, a positive gradient in potential temperature  
670 (272 K at the ground vs. 278 K at the balloon, **Figure 5c**) indicated a stably stratified boundary  
671 layer. Specific humidity was uniform (3.2–3.8 g kg<sup>-1</sup>), while  $N_{150}$  was lower than in Case I (3–10  
672 cm<sup>-3</sup>) with higher relative variability, likely influenced by low counting statistics at these low  
673 concentrations. Overall, mixing conditions in Case III were similar to Case I, but sampling  
674 occurred partly within or below a drizzling low-level cloud.

675 Back-trajectory analysis (**Figure 6, Case III**) showed that air masses at the altitudes of ground,  
676 balloon, and Zeppelin Observatory followed the same 48-h path from the ice-free ocean south  
677 of Svalbard. Vertical trajectory heights indicate shared transport history and influence by the  
678 same emission sources, consistent with Case I.

679 In line with the lower aerosol number concentrations, offline measurements of chemical  
680 constituents were also generally lower than in the previous cases. Furthermore, major

681 inorganic ions (**Figure 5c**) were generally similar at the ground and balloon ( $\text{Cl}_{\text{aer}}^-$ : 289 &  
682 252  $\text{ng m}^{-3}$ ;  $\text{SO}_{4\text{aer}}^{2-}$ : 66 & 59  $\text{ng m}^{-3}$ ;  $\text{K}_{\text{aer}}^+$ : 23 & 20  $\text{ng m}^{-3}$ ), with  $\text{Na}_{\text{aer}}^+$  (53 & 35  $\text{ng m}^{-3}$ )  
683 somewhat higher at the ground. At the Zeppelin Observatory, only  $\text{Na}_{\text{aer}}^+$  exceeded the  
684 detection limit, with a concentration of 38  $\text{ng m}^{-3}$ , very similar to the value observed at the  
685 balloon. This consistency indicates a rather mixed boundary layer. Creamean et al. (2021)  
686 analyzed three years of Arctic aerosol vertical distributions using a tethered balloon in Alaska  
687 and found that, when a uniform aerosol distribution below clouds was observed, it primarily  
688 occurred in autumn, aligning well with Case III.

689 Interestingly, despite the same levels of major inorganic ions, some chemical constituents  
690 exhibited increased concentrations at higher altitudes. These included major  
691 monosaccharides bound within CCHO (ground & balloon:  $\text{Glc}_{\text{CCHO,aer}}$ : 12.6 & 34  $\text{ng m}^{-3}$ ;  
692  $\text{Xyl}_{\text{CCHO,aer}}$ : 0.57 & 4.4  $\text{ng m}^{-3}$ ;  $\text{Ara}_{\text{CCHO,aer}}$ : below detection limit & 0.97  $\text{ng m}^{-3}$ ), as well as  
693 oxalate<sub>aer</sub> (5.5 & 24  $\text{ng m}^{-3}$ ),  $\text{Ca}_{\text{aer}}^{2+}$  (47 & 187  $\text{ng m}^{-3}$ ), and  $\text{Mg}_{\text{aer}}^{2+}$  (0.97 & 2.6  $\text{ng m}^{-3}$ ). These  
694 elevated concentrations cannot be explained by direct local sea spray emissions or remote  
695 source contributions alone, suggesting the involvement of cloud-related enrichment and  
696 transformation processes.

697 Soluble  $\text{Ca}_{\text{aer}}^{2+}$  and  $\text{Mg}_{\text{aer}}^{2+}$  possibly derived from preexisting organic structures in SSA,  
698 becoming soluble and detectable after chemical aging. OM-bound  $\text{Ca}^{2+}$ , as already found in  
699 Antarctic SSA (Su et al., 2023), may originate from SML-derived polysaccharide gels such as  
700 TEPs, and airborne algal cells or fragments, which can release  $\text{Ca}^{2+}$  and  $\text{Mg}^{2+}$  through gel  
701 dispersion or cell dissolution under the acidic conditions of chemically aged SSA aerosol  
702 particles (Aller et al., 2017; Angle et al., 2021; Orellana and Leck, 2015; van Pinxteren et al.,  
703 2022; Trainic et al., 2018; Zhu et al., 2014). Since these particles were sampled in cloud water,  
704 which contains abundant TEP (van Pinxteren et al., 2022), this mechanism may also explain  
705 the elevated CCHO concentrations.  $\text{Ca}_{\text{aer}}^{2+}$  can form complexes with oxalate<sub>aer</sub> (Furukawa and  
706 Takahashi, 2011), and oxalic acid increases hygroscopicity, potentially accounting for the high  
707 values observed at the balloon in Case III. In addition, secondary in-situ atmospheric or  
708 microbial origins, particularly in the aqueous phase, may contribute to CCHO<sub>aer</sub> and oxalate<sub>aer</sub>  
709 and is discussed in the following section.

710 In summary, Case III demonstrates that certain SSA constituents can vary with altitude due to  
711 atmospheric processing following primary emissions and vertical transport.

712 Together, the three cases demonstrate that meteorological conditions can lead to similar,  
713 lower, or higher concentrations of the investigated chemical constituents across different  
714 altitudes. The three cases show that meteorological conditions can produce similar, lower, or  
715 higher chemical concentrations at different altitudes. Porter et al. (2022) observed similar  
716 patterns for ice-nucleating particles at the North Pole. They combined their measurements  
717 with trajectory analyses and heat sensitivity tests to conclude on aerosol sources. While this  
718 effect-based approach gives insights into particle properties, direct chemical analyses, as  
719 performed in this study, can further enhance certainty about particle origin and composition  
720 relevant for cloud formation.

721 **3.3 Factors affecting SSA constituents beyond local sea-air transfer**

722 *Long-range transport and size-dependent deposition*

723 SSA particles originate from both local and remote marine regions. However, our sampling  
724 methods make it challenging to determine the relative contribution of long-range transported  
725 SSA constituents, particularly when a local marine source, such as the Kongsfjorden is adjacent  
726 to the sampling site and may dominate other marine emissions.

727 As demonstrated in Case II, long-range transport of SSA can become dominant when air  
728 masses at elevated altitudes are decoupled from those at the ground. In this case, vertical and  
729 horizontal trajectory analysis suggests that the measured SSA constituents may have been  
730 emitted and incorporated into the atmosphere approximately 48 hours earlier over the  
731 Barents Sea, near Franz Josef Land. Typical removal processes of supermicron particles, such  
732 as dry and wet deposition or cloud droplet activation, likely reduced the atmospheric  
733 concentrations of major inorganic ions and  $\text{CCHO}_{\text{aer}}$  by one to two orders of magnitude before  
734 the arrival of the air masses in Ny-Ålesund (**Figure 5b**).

735 In several balloon-borne TSP filter samples, an elevated  $\text{CCHO}_{\text{aer}}/\text{Na}^+_{\text{aer}}$  ratio was observed,  
736 most notably on 24 Sep 2021; 03 Oct 2021 (Case III) and 03 Apr 2022 (see **Figure 2d**). These  
737 values far exceeded both ground-based aerosol measurements from this study and previously  
738 reported values (Zeppenfeld et al., 2021, 2023), particularly for supermicron SSA particles that  
739 dominate the TSP mass. A slight increase of this ratio may be explained by a longer  
740 atmospheric residence time of these particles. This leads to a relative reduction of  
741 supermicron aerosol particles, typically dominated by sea salt (O'Dowd and de Leeuw, 2007),  
742 through deposition (Croft et al., 2009; Hoppel et al., 2002). In contrast, submicron aerosol  
743 particles, which are rich in surface-active CCHO, remain. This process could lead to a shift of  
744 the  $\text{CCHO}_{\text{aer}}/\text{Na}^+_{\text{aer}}$  ratios more characteristic of submicron than supermicron particles in the  
745 TSP samples of this study, as seen in Case II.

746 However, for the three cases with the most pronounced increases in  $\text{CCHO}_{\text{aer}}/\text{Na}^+_{\text{aer}}$  ratios in  
747 TSP at higher altitudes (24 Sep 2021; 03 Oct 2021; 03 Apr 2022), absolute  $\text{CCHO}_{\text{aer}}$   
748 concentrations were also elevated (compare **Figures 2b and 2d**). Such increases in absolute  
749 concentrations cannot be explained by the selective removal of supermicron particles as  
750 hypothesized above. This raises the question of whether the observed  $\text{CCHO}_{\text{aer}}$  concentrations

751 could result from the long-range transport of SSA compounds from a distant marine source  
752 with significantly higher CCHO levels than the local Kongsfjorden.

753 Model simulations using FESOM2.1-REcoM3 (Gürses et al., 2023) (**Figure S6**) and field data  
754 (Assmy et al., 2023; Feltracco et al., 2021; Grosse et al., 2021; Wietz et al., 2024) confirm that  
755 the eastern Fram Strait as well as coastal Svalbard waters are productive and polysaccharide-  
756 rich regions. While the FESOM2.1-REcoM3 model does not resolve the SML separately,  
757 previous studies have shown significant CCHO enrichment in this layer (Compiano et al., 1993;  
758 Engel and Galgani, 2016; Gao et al., 2012; Zäncker et al., 2021), particularly in the productive  
759 marginal ice zone (Zeppenfeld et al., 2023). However, in cases of high CCHO<sub>aer</sub> at higher  
760 altitudes in this study, air mass trajectories did not pass over any of these productive marine  
761 regions within 48 hours before reaching Svalbard (**Figure S7**). These findings suggest that long-  
762 range transport of SSA from more productive remote marine sources is unlikely to explain the  
763 elevated CCHO<sub>aer</sub> concentrations at elevated altitudes within the lower troposphere in Ny-  
764 Ålesund, further supporting a predominantly local source or atmospheric in-situ formation.

765 In summary, while long-range transport of SSA constituents at elevated altitudes appears  
766 relevant in cases of decoupled atmospheric layers such as in Case II, it may not explain the  
767 significantly higher CCHO<sub>aer</sub> concentrations at high altitudes compared to ground levels.  
768 Instead, in-situ formation of CCHO<sub>aer</sub> could be a more plausible explanation for these  
769 observations.

770

#### 771 ***Atmospheric in-situ formation of marine CCHO<sub>aer</sub>***

772 Bacteria can be transported into and persist in the Arctic atmosphere (Jensen et al., 2022;  
773 Šantl-Temkiv et al., 2018), with sources including terrestrial environments and surface  
774 seawater, particularly the SML (Aller et al., 2005). Our complementary microbiological  
775 sampling during our campaign supported such dynamics by detecting diverse marine bacteria  
776 in aerosol particles (Wietz et al., 2025). Some aerosolized taxa, for instance *Polaribacter*,  
777 encode multiple genes for CCHO metabolism (Avci et al., 2020) and consistently occur in both  
778 Kongsfjorden seawater and atmosphere during the spring bloom (Feltracco et al., 2021). These  
779 observations might underpin microbial CCHO transformations in the atmosphere, for instance  
780 the production of polysaccharide-based gels as protection against temperature fluctuations,  
781 salinity changes, and desiccation (Aller et al., 2005; Ramasamy et al., 2023; Šantl-Temkiv et al.,

782 2022). Under highly humid conditions, especially in the presence of liquid water (such as in  
783 Case III), airborne bacteria can become metabolically active (Ervens and Amato, 2020;  
784 Haddrell and Thomas, 2017). Atmospheric OM formation, including CCHO, through microbial  
785 activity has been documented for cloud water and aerosol particles (Bianco et al., 2019; Klein  
786 et al., 2016; Matulová et al., 2014). [Although substantial uncertainties remain, Zeppenfeld et  
787 al. \(2021\) estimated, depending on parameter choice, residence times between 20 minutes  
788 and several hundred hours during which measurable microbial transformation of  
789 carbohydrates in the atmosphere may occur.](#) Consequently, metabolically active bacteria in  
790 the atmosphere could explain the increased CCHO<sub>aer</sub> concentrations observed within or near  
791 drizzling clouds in Case III of this study.

#### 792 ***CCHO<sub>aer</sub> versus oxalate<sub>aer</sub>: Co-production or atmospheric processing?***

793 Since both combined glucose and combined xylose were consistently detected in CCHO<sub>aer</sub> of  
794 nearly all aerosol samples, we examined their correlation with other atmospheric chemical  
795 parameters. We observed a strong correlation between atmospheric xylose in CCHO<sub>aer</sub> and  
796 oxalate<sub>aer</sub> with an R=0.78 (p<0.001) across all sampling locations and heights (**Figure 7**).  
797 Oxalate, the ionic form of oxalic acid, is the most abundant dicarboxylic acid in aerosol  
798 particles (Kerminen et al., 1999; Rinaldi et al., 2011), with atmospheric concentrations in this  
799 study between <1 and 67 ng m<sup>-3</sup>. The strong correlation raised the question of whether oxalic  
800 acid could be chemically linked to combined carbohydrates in aerosol particles.

801 Oxalate<sub>aer</sub> is known to originate from several primary sources and secondary formation  
802 pathways in both terrestrial and anthropogenic environments (Kawamura and Bikkina, 2016;  
803 Yang et al., 2022). In remote marine environments, the atmospheric formation of oxalic acid  
804 was proposed by Warneck (2003) through the aqueous-phase oxidation of glyoxal and  
805 glycolaldehyde, a process also investigated by field measurements inside and above marine  
806 clouds (Crahan et al., 2004; Sorooshian et al., 2007) and modeling (Herrmann et al., 2005;  
807 Tilgner and Herrmann, 2010). The possible aqueous-phase formation was supported by Case  
808 III of this study, where higher oxalate<sub>aer</sub> concentrations were observed within and in vicinity of  
809 clouds compared to ground level. In contrast, in the drier conditions of Cases I and II, oxalate<sub>aer</sub>  
810 levels remained vertically uniform. Additionally, since overall oxalate<sub>aer</sub> levels at the Old Pier  
811 (1.1–10.1 ng m<sup>-3</sup>; mean=4.3±3.5 ng m<sup>-3</sup>) were relatively low compared to the more inland

812 Winch (<1–58 ng m<sup>-3</sup>; mean=19.8±16.2 ng m<sup>-3</sup>) and elevated altitudes samples (4.6–67 ng m<sup>-3</sup>;  
813 mean=29.6±17.8 ng m<sup>-3</sup>), direct primary oceanic emission was likely not its dominant source.

814

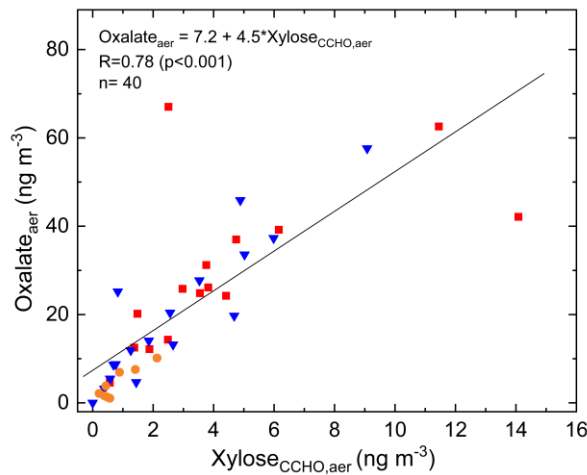


**Figure 7.** Atmospheric oxalate as a function of xylose in CCHO<sub>aer</sub> (R=0.78; p<0.001) measured in TSP from the Old Pier (orange circles), the winch site (blue triangles) and at elevated altitudes (red squares).

823 But what are the precursors of glyoxal and glycolaldehyde, the precursors of oxalic acid  
824 precursors? While Warneck (2003) suggested that the anthropogenic volatile organic  
825 compounds acetylene and ethene can be transformed to atmospheric glyoxal, other studies  
826 suggest the photochemical degradation of marine OM (McNeill, 2015; Sinreich et al., 2010;  
827 Turekian et al., 2003; Zhou et al., 2014), with oligo- and polysaccharides representing a known  
828 subclass. Although not explicitly measured in this study, previous findings have shown that  
829 both CCHO<sub>aer</sub> (Leck et al., 2013; Zeppenfeld et al., 2021, 2023) and oxalate<sub>aer</sub> (Guo et al., 2016;  
830 Rinaldi et al., 2011; Turekian et al., 2003) are present across both the accumulation and coarse  
831 size modes. However, no consistently dominant size mode has been identified, which may  
832 support a common mechanism of formation or similar atmospheric processing pathways.

833 Here, based on known chemical reactions, we propose possible atmospheric pathways linking  
834 xylose-containing oligo- and polysaccharides as the precursors to oxalate as the final product  
835 (**Figure 8**). The initial depolymerization of CCHO presumably occurs either via enzymatic  
836 degradation, e.g. by glycoside hydrolases, or acid hydrolysis (Panagiotopoulos and Sempéré,

837 2005), both of which are plausible in the atmospheric context. Active microbial enzymes have  
 838 been detected in SSA, often exhibiting activities 1–2 orders of magnitude higher than in bulk  
 839 seawater (Malfatti et al., 2019). Additionally, SSA particles are known for reaching very low pH  
 840 levels within minutes after their emissions due to the uptake and reactions with acidic gases,  
 841 as well as water loss (Angle et al., 2022, 2021). Furthermore, although not explicitly  
 842 investigated in an atmospheric context, Zhu et al. (2023) observed rapid depolymerization of  
 843 xylose-containing oligosaccharides into the monosaccharide xylose within minutes in a  
 844 UV/H<sub>2</sub>O<sub>2</sub> system, which generates hydroxyl radicals.

845  
846  
847  
848  
849  
850  
851  
852  
853  
854

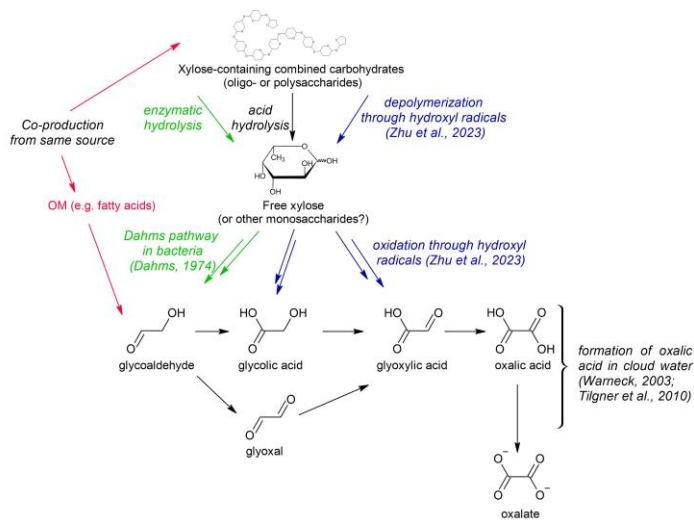


**Figure 8.** Possible pathways for the formation of atmospheric oxalate from xylose in combined carbohydrates in marine aerosol particles.

855 With one exception, free xylose was never detected in any aerosol sample of this study. This  
 856 suggests two possible explanations. First, xylose may have remained bound within the CCHO<sub>aer</sub>  
 857 fraction and was not released into its free form. In this case, it would indicate co-emission  
 858 without a chemical pathway leading to oxalate. Second, free xylose may have been rapidly  
 859 processed in the atmosphere via reactions described below.

860 Two potential pathways may link monomeric xylose to precursors of Warneck's oxalate  
 861 formation: (1) a follow-up reaction with hydroxyl radicals, where the pyranose ring of xylose  
 862 is cleaved after the more susceptible glycosidic bonds have been readily broken. Zhu et al.

863 (2023) observed glycolic acid and glyoxylic acid among other products following the UV/H<sub>2</sub>O<sub>2</sub>  
864 treatment of xylooligosaccharides. (2) Bacterial metabolism via the Dahms pathway  
865 converting free xylose into pyruvate and glycolaldehyde (Dahms, 1974). However, only few  
866 bacteria encode this pathway; and it is highly questionable whether these occur in sufficient  
867 atmospheric concentrations for a measurable effect.

868 One indication that direct formation from xylose-containing oligo- and polysaccharides cannot  
869 be the sole source of atmospheric oxalate in the marine environment is the discrepancy in  
870 concentrations: atmospheric oxalate levels were seven times higher than those of combined  
871 xylose. This confirms the involvement of additional precursors or a co-production/co-emission  
872 of combined xylose with gaseous precursors, such as isoprene (Carlton et al., 2009; Kawamura  
873 and Bikkina, 2016), or other primary marine organic matter, such as phytoplankton-derived  
874 fatty acids (Kawamura et al., 1996<sup>ba</sup>, <sup>ba</sup>) undergoing photo-oxidation. Further targeted  
875 laboratory and modeling studies are needed for clarity.

## 876 **4. Summary and Atmospheric Implications**

877 In autumn 2021 and spring 2022, we performed balloon-borne measurements of major SSA  
878 constituents at Ny-Ålesund (Svalbard). Our evidence demonstrated that both sodium and  
879 marine CCHO reach elevated altitudes within the boundary layer, and even the free  
880 troposphere as part of aerosol particles. The relationship between ground-level and high-  
881 altitude measurements was strongly influenced by meteorological conditions and the mixing  
882 state of the lower atmosphere, as discussed in three representative cases. Long-range  
883 transport of  $\text{Na}^+_{\text{aer}}$  and  $\text{CCHO}_{\text{aer}}$  from remote marine sources is presumably relevant for high-  
884 altitude measurements, especially when the upper air masses were decoupled from the  
885 ground. However, in cases of a well-mixed lower atmosphere, the local marine source (here,  
886 the Kongsfjorden) was the dominant contributor for atmospheric  $\text{Na}^+_{\text{aer}}$  and  $\text{CCHO}_{\text{aer}}$ . Under  
887 very humid conditions particularly in the presence of liquid precipitating clouds, in-situ  
888 formation of  $\text{CCHO}_{\text{aer}}$  was observed, possibly linked to microbial metabolism. To establish  
889 more generalizable patterns, we recommend further field studies using airborne platforms.

890 The significant correlation between combined xylose within  $\text{CCHO}_{\text{aer}}$ , and oxalate<sub>aer</sub> suggests  
891 underlying pathways for oxalic acid formation from combined xylose and other  
892 monosaccharide units within  $\text{CCHO}_{\text{aer}}$ ; alternatively, a co-production of xylose-containing  
893 oligo- and polysaccharides alongside oxalate precursors.

894 Cloud condensation nuclei and ice-nucleating particles are key drivers in cloud formation,  
895 influencing radiative and precipitation properties and, consequently, climate processes.  
896 Considerable uncertainties remain regarding the origin and chemical composition of these  
897 particles, particularly in remote Arctic regions, which affects the accuracy of climate models.  
898 Since marine polysaccharides have been identified as relevant ice-nucleating molecules in the  
899 remote marine atmosphere (Hartmann et al., 2025), our findings have implications for cloud  
900 microphysics, especially given that these carbohydrates are transported to altitudes relevant  
901 for cloud formation. Furthermore, atmospheric processing, as observed here, may alter the  
902 ice-nucleating properties of these macromolecules, potentially creating new ice-nucleating  
903 particles in-situ or deactivating existing ones.

904 As the Arctic continues to change, expanding ice-free ocean areas will serve as emission  
905 sources for SSA particles, influencing cloud properties, and finally the radiative budget.

906 Consequently, our findings contribute to an improved understanding of the complex interplay  
907 of environmental processes resulting in Arctic amplification (Wendisch et al., 2017, 2023).

## 908 **Author contributions**

909 SZ wrote the manuscript with input from all co-authors. SZ, JS, CP, HS, BW, MW, and MvP  
910 collected field samples in Ny-Ålesund. HS and BW served as principal investigators for balloon  
911 operations during the field campaign. SZ conducted the laboratory carbohydrate analyses and  
912 data processing. MZ and AB carried out the FESOM2.1-REcoM3 simulations. KE assessed cloud  
913 conditions for the case studies using remote sensing data. All co-authors reviewed and  
914 commented on the manuscript.

915

## 916 **Acknowledgments**

917 We would like to express our gratitude to Kings Bay and the AWIPEV staff, with special thanks  
918 to the station leader Grégory Tran, for their invaluable support to make this field study  
919 possible. We furthermore thank the AWIPEV station's scientific staff in ensuring the  
920 availability of high-quality meteorological data. In this context, we like to give special thanks  
921 to Fieke Rader and Marion Maturilli. The cloud observations were taken within the project  
922 AWIPEV\_0016.

923 We also thank the scientific team at the Zeppelin Observatory from NILU and NPI, with special  
924 appreciation to Wenche Aas, for their dedicated work in monitoring aerosol data.

925 Furthermore, we acknowledge the entire BELUGA team for their contributions during both  
926 the autumn 2021 and spring 2022 campaigns, with special thanks to Thomas Conrath. We also  
927 thank Michel Michalkow for preprocessing the CAMP and standard meteorological data  
928 collected at BELUGA as part of his Master's thesis. We are grateful to René Rabe for preparing  
929 the campaign equipment and to Leon Schmidt for conducting the chemical analysis of  
930 inorganic ions.

931 For the FESOM2.1-REcoM3 simulation for this research, the authors gratefully acknowledge  
932 the computing time granted by the Resource Allocation Board and provided on the  
933 supercomputer Lise and Emmy at NHR@ZIB and NHR@Göttingen as part of the NHR

934 infrastructure. The calculations for this research were conducted with computing resources  
935 under the project hbk00084.

936 This research has been supported by the Deutsche Forschungsgemeinschaft (DFG, German  
937 Research Foundation, project no. 268020496-TRR 172) within the Transregional Collaborative  
938 Research Center “Arctic Amplification: Climate Relevant Atmospheric and SurfaCe Processes,  
939 and Feedback Mechanisms (AC)3” in subprojects A02, B04, C03 and E02. MW was supported  
940 by the DFG Priority Program SPP 1158 “Antarctic Research with comparative investigations in  
941 Arctic ice areas” (grant 522416631). We thank Johannes Röttenbacher for his constructive  
942 feedback on the manuscript.

943

#### 944 **Competing interests**

945 All authors declare no financial or non-financial competing interests. Some authors are  
946 members of the editorial board of ACP.

947

#### 948 **Data availability**

949 Chemical data from offline TSP filters are publicly available in PANGAEA for seawater  
950 (Zeppenfeld and Schmidt, 2025) and aerosol particles (Zeppenfeld et al., 2025). The  
951 microwave radiometer LWP and IWV data are available in PANGAEA (Ebell and Ritter, 2022).  
952 The Cloudnet classification and ice water content products (Ebell et al., 2025) can be  
953 downloaded via the ACTRIS Cloudnet data portal (<https://cloudnet.fmi.fi>).

## 954 References

- 955 Aas, W., Berglen, T. F., Eckhardt, S., Fiebig, M., Solberg, S., and Yttri, K. E.: Monitoring of long-range transported air pollutants  
956 in Norway. Annual Report 2021., NILU, 2022.
- 957 Aas, W., Eckhardt, S., Solberg, S., and Yttri, K. E.: Monitoring of long-range transported air pollutants in Norway. Annual Report  
958 2022., NILU, 2023.
- 959 Akansu, E. F., Dahlke, S., Siebert, H., and Wendisch, M.: Evaluation of methods to determine the surface mixing layer height  
960 of the atmospheric boundary layer in the central Arctic during polar night and transition to polar day in cloudless and cloudy  
961 conditions, *Atmospheric Chemistry and Physics*, 23, 15473–15489, <https://doi.org/10.5194/acp-23-15473-2023>, 2023.
- 962 Aller, J. Y., Kuznetsova, M. R., Jahns, C. J., and Kemp, P. F.: The sea surface microlayer as a source of viral and bacterial  
963 enrichment in marine aerosols, *Journal of Aerosol Science*, 36, 801–812, <https://doi.org/10.1016/j.jaerosci.2004.10.012>,  
964 2005.
- 965 Aller, J. Y., Radway, J. C., Kiltthau, W. P., Bothe, D. W., Wilson, T. W., Vaillancourt, R. D., Quinn, P. K., Coffman, D. J., Murray,  
966 B. J., and Knopf, D. A.: Size-resolved characterization of the polysaccharidic and proteinaceous components of sea spray  
967 aerosol, *Atmospheric Environment*, 154, 331–347, <https://doi.org/10.1016/j.atmosenv.2017.01.053>, 2017.
- 968 Alpert, P. A., Kiltthau, W. P., O'Brien, R. E., Moffet, R. C., Gilles, M. K., Wang, B., Laskin, A., Aller, J. Y., and Knopf, D. A.: Ice-  
969 nucleating agents in sea spray aerosol identified and quantified with a holistic multimodal freezing model, *Science Advances*,  
970 8, eabq6842, <https://doi.org/10.1126/sciadv.abq6842>, 2022.
- 971 Aluwihare, L. I., Repeta, D. J., and Chen, R. F.: A major biopolymeric component to dissolved organic carbon in surface sea  
972 water, *Nature*, 387, 166–169, <https://doi.org/10.1038/387166a0>, 1997.
- 973 Amore, A., Giardi, F., Becagli, S., Caiazzo, L., Mazzola, M., Severi, M., and Traversi, R.: Source apportionment of sulphate in  
974 the High Arctic by a 10 yr-long record from Gruebadet Observatory (Ny-Ålesund, Svalbard Islands), *Atmospheric  
975 Environment*, 270, 118890, <https://doi.org/10.1016/j.atmosenv.2021.118890>, 2022.
- 976 Angle, K., Grassian, V. H., and Ault, A. P.: The rapid acidification of sea spray aerosols, *Physics today*, 75, 58–59,  
977 <https://doi.org/10.1063/PT.3.4926>, 2022.
- 978 Angle, K. J., Crocker, D. R., Simpson, R. M. C., Mayer, K. J., Garofalo, L. A., Moore, A. N., Garcia, S. L. M., Or, V. W., Srinivasan,  
979 S., Farhan, M., Sauer, J. S., Lee, C., Pothier, M. A., Farmer, D. K., Martz, T. R., Bertram, T. H., Cappa, C. D., Prather, K. A., and  
980 Grassian, V. H.: Acidity across the interface from the ocean surface to sea spray aerosol, *PNAS*, 118, 1–6,  
981 <https://doi.org/10.1073/pnas.2018397118>, 2021.
- 982 Arnosti, C., Wietz, M., Brinkhoff, T., Hehemann, J.-H., Probandt, D., Zeugner, L., and Amann, R.: The Biogeochemistry of  
983 Marine Polysaccharides: Sources, Inventories, and Bacterial Drivers of the Carbohydrate Cycle, *Ann Rev Mar Sci*, 13, 81–108,  
984 <https://doi.org/10.1146/annurev-marine-032020-012810>, 2021.
- 985 Assmy, P., Cecilie Kvernvik, A., Hop, H., Hoppe, C. J. M., Chierici, M., David T., D., Duarte, P., Fransson, A., García, L. M., Patula,  
986 W., Kwaśniewski, S., Maturilli, M., Pavlova, O., Tatarek, A., Wiktor, J. M., Wold, A., Wolf, K. K. E., and Bailey, A.: Seasonal  
987 plankton dynamics in Kongsfjorden during two years of contrasting environmental conditions, *Progress in Oceanography*,  
988 213, 102996, <https://doi.org/10.1016/j.pocean.2023.102996>, 2023.
- 989 Avci, B., Krüger, K., Fuchs, B. M., Teeling, H., and Amann, R. I.: Polysaccharide niche partitioning of distinct *Polaribacter* clades  
990 during North Sea spring algal blooms, *ISME J*, 14, 1369–1383, <https://doi.org/10.1038/s41396-020-0601-y>, 2020.
- 991 Barthelmeß, T., Cristi, A., Deppeler, S., Safi, K., Sellegri, K., Law, C. S., and Engel, A.: Pronounced Diel Cycling of Dissolved  
992 Carbohydrates and Amino Acids in the Surface Ocean and across Diverse Regimes, *Environ. Sci. Technol.*, 59, 419–429,  
993 <https://doi.org/10.1021/acs.est.4c00491>, 2025.
- 994 Becker, S., Tebben, J., Coffinet, S., Wiltshire, K., Iversen, M. H., Harder, T., Hinrichs, K.-U., and Hehemann, J.-H.: Laminarin is  
995 a major molecule in the marine carbon cycle, *PNAS*, 117, 6599–6607, <https://doi.org/10.1073/pnas.1917001117>, 2020.
- 996 Bianco, A., Deguillaume, L., Chaumerliac, N., Vaïtilingom, M., Wang, M., Delort, A.-M., and Bridoux, M. C.: Effect of  
997 endogenous microbiota on the molecular composition of cloud water: a study by Fourier-transform ion cyclotron resonance  
998 mass spectrometry (FT-ICR MS), *Sci Rep*, 9, 1–12, <https://doi.org/10.1038/s41598-019-44149-8>, 2019.
- 999 Bischof, K., Convey, P., Duarte, P., Gattuso, J.-P., Granberg, M., Hop, H., Hoppe, C., Jiménez, C., Lisitsyn, L., Martínez, B.,  
1000 Røleda, M. Y., Thor, P., Wiktor, J. M., and Gabrielsen, G. W.: Kongsfjorden as Harbinger of the Future Arctic: Knowns,  
1001 Unknowns and Research Priorities, in: *The Ecosystem of Kongsfjorden, Svalbard*, edited by: Hop, H. and Wiencke, C., Springer  
1002 International Publishing, Cham, 537–562, [https://doi.org/10.1007/978-3-319-46425-1\\_14](https://doi.org/10.1007/978-3-319-46425-1_14), 2019.
- 1003 Bivand, R., Pebesma, E., and Gomez-Rubio, V.: *Applied spatial data analysis with R*, Springer, 2013.
- 1004 Bivand, R., Keitt, T., and Rowlingson, B.: *rgdal: Bindings for the “Geospatial” Data Abstraction Library*, R package version 1.5-  
1005 32, 2022.

1006 Borch, N. H. and Kirchman, D. L.: Concentration and composition of dissolved combined neutral sugars (polysaccharides) in  
1007 seawater determined by HPLC-PAD, *Marine Chemistry*, 57, 85–95, [https://doi.org/10.1016/S0304-4203\(97\)00002-9](https://doi.org/10.1016/S0304-4203(97)00002-9), 1997.

1008 Brownrigg, M. R.: Package ‘mapdata’, R package version 2.3.1, 2013.

1009 Brownrigg, M. R.: maps: Draw Geographical Maps, R package version 3.4.2, 2023.

1010 Browse, J., Carslaw, K. S., Mann, G. W., Birch, C. E., Arnold, S. R., and Leck, C.: The complex response of Arctic aerosol to sea-  
1011 ice retreat, *Atmospheric Chemistry and Physics*, 14, 7543–7557, <https://doi.org/10.5194/acp-14-7543-2014>, 2014.

1012 Burns, W. G., Marchetti, A., and Zierovogel, K.: Enhanced formation of transparent exopolymer particles (TEP) under  
1013 turbulence during phytoplankton growth, *J Plankton Res*, 41, 349–361, <https://doi.org/10.1093/plankt/fbz018>, 2019.

1014 Burrows, S. M., Ogunro, O., Frossard, A., Russell, L. M., Rasch, P. J., and Elliott, S.: A Physically Based Framework for Modelling  
1015 the Organic Fractionation of Sea Spray Aerosol from Bubble Film Langmuir Equilibria, *Atmospheric Chemistry and Physics*,  
1016 14(24):13601–13629, <https://doi.org/10.5194/acp-14-13601-2014>, 2014.

1017 Cai, Q., Wang, J., Beletsky, D., Overland, J., Ikeda, M., and Wan, L.: Accelerated decline of summer Arctic sea ice during 1850–  
1018 2017 and the amplified Arctic warming during the recent decades, *Environ. Res. Lett.*, 16, 034015,  
1019 <https://doi.org/10.1088/1748-9326/abdb5f>, 2021.

1020 Carlton, A. G., Wiedinmyer, C., and Kroll, J. H.: A review of Secondary Organic Aerosol (SOA) formation from isoprene,  
1021 *Atmospheric Chemistry and Physics*, 9, 4987–5005, <https://doi.org/10.5194/acp-9-4987-2009>, 2009.

1022 Carslaw, D. C. and Ropkins, K.: openair --- An R package for air quality data analysis, *Environmental Modelling & Software*,  
1023 27–28, 52–61, 2012.

1024 Chang, L., Song, S., Feng, G., Zhang, Y., and Gao, G.: Assessment of the Uncertainties in Arctic Low-Level Temperature  
1025 Inversion Characteristics in Radio Occultation Observations, *IEEE Transactions on Geoscience and Remote Sensing*, 55, 1793–  
1026 1803, <https://doi.org/10.1109/TGRS.2016.2633461>, 2017.

1027 Chi, J. W., Li, W. J., Zhang, D. Z., Zhang, J. C., Lin, Y. T., Shen, X. J., Sun, J. Y., Chen, J. M., Zhang, X. Y., Zhang, Y. M., and Wang,  
1028 W. X.: Sea salt aerosols as a reactive surface for inorganic and organic acidic gases in the Arctic troposphere, *Atmospheric  
1029 Chemistry and Physics*, 15, 11341–11353, <https://doi.org/10.5194/acp-15-11341-2015>, 2015.

1030 Compiano, A.-M., Romano, J.-C., Garabetian, F., Laborde, P., and de la Giraudière, I.: Monosaccharide composition of  
1031 particulate hydrolysable sugar fraction in surface microlayers from brackish and marine waters, *Marine Chemistry*, 42, 237–  
1032 251, [https://doi.org/10.1016/0304-4203\(93\)90015-G](https://doi.org/10.1016/0304-4203(93)90015-G), 1993.

1033 Crahan, K. K., Hegg, D., Covert, D. S., and Jonsson, H.: An exploration of aqueous oxalic acid production in the coastal marine  
1034 atmosphere, *Atmospheric Environment*, 38, 3757–3764, <https://doi.org/10.1016/j.atmosenv.2004.04.009>, 2004.

1035 Creamean, J. M., de Boer, G., Telg, H., Mei, F., Dexheimer, D., Shupe, M. D., Solomon, A., and McComiskey, A.: Assessing the  
1036 vertical structure of Arctic aerosols using balloon-borne measurements, *Atmospheric Chemistry and Physics*, 21, 1737–1757,  
1037 <https://doi.org/10.5194/acp-21-1737-2021>, 2021.

1038 Croft, B., Lohmann, U., Martin, R. V., Stier, P., Wurzel, S., Feichter, J., Posselt, R., and Ferrachat, S.: Aerosol size-dependent  
1039 below-cloud scavenging by rain and snow in the ECHAM5-HAM, *Atmospheric Chemistry and Physics*, 9, 4653–4675,  
1040 <https://doi.org/10.5194/acp-9-4653-2009>, 2009.

1041 Cunliffe, M. and Wurl, O.: Guide to best practices to study the ocean’s surface., *Marine Biological Association of the United  
1042 Kingdom for SCOR*, 2014.

1043 Dahms, A. S.: 3-Deoxy-D-pentulose acid aldolase and its role in a new pathway of D-xylose degradation, *Biochemical and  
1044 Biophysical Research Communications*, 60, 1433–1439, [https://doi.org/10.1016/0006-291X\(74\)90358-1](https://doi.org/10.1016/0006-291X(74)90358-1), 1974.

1045 Dekhtyareva, A., Holmén, K., Maturilli, M., Hermansen, O., and Gravensen, R.: Effect of seasonal mesoscale and microscale  
1046 meteorological conditions in Ny-Ålesund on results of monitoring of long-range transported pollution, *Polar Research*, 2018.

1047 DeMott, P. J., Hill, T. C. J., McCluskey, C. S., Prather, K. A., Collins, D. B., Sullivan, R. C., Ruppel, M. J., Mason, R. H., Irish, V. E.,  
1048 Lee, T., Hwang, C. Y., Rhee, T. S., Snider, J. R., McMeeking, G. R., Dhaniyala, S., Lewis, E. R., Wentzell, J. J. B., Abbatt, J., Lee,  
1049 C., Sultana, C. M., Ault, A. P., Axson, J. L., Martinez, M. D., Venero, I., Santos-Figueroa, G., Stokes, M. D., Deane, G. B., Mayol-  
1050 Bracero, O. L., Grassian, V. H., Bertram, T. H., Bertram, A. K., Moffett, B. F., and Franc, G. D.: Sea spray aerosol as a unique  
1051 source of ice nucleating particles, *PNAS*, 113, 5797–5803, <https://doi.org/10.1073/pnas.1514034112>, 2016.

1052 Dusek, U., Frank, G. P., Hildebrandt, L., Curtius, J., Schneider, J., Walter, S., Chand, D., Drewnick, F., Hings, S., Jung, D.,  
1053 Borrmann, S., and Andreae, M. O.: Size Matters More Than Chemistry for Cloud-Nucleating Ability of Aerosol Particles,  
1054 *Science*, 312, 1375–1378, <https://doi.org/10.1126/science.1125261>, 2006.

1055 Ebell, K. and Ritter, C.: HATPRO microwave radiometer measurements at AWIPEV, Ny-Ålesund (2019–2021), *PANGAEA*,  
1056 <https://doi.org/10.1594/PANGAEA.943004>, 2022.

1057 Ebell, K., Maturilli, M., Ritter, C., and O’Connor, E.: Custom collection of classification, and ice water content data from Ny-  
1058 Ålesund between 27 Sep and 12 Nov 2021, ACTRIS Cloud remote sensing data centre unit (CLU),  
1059 <https://doi.org/10.60656/5598100185854c01>, 2025.

1060 Egerer, U., Ehrlich, A., Gottschalk, M., Griesche, H., Neggers, R. A. J., Siebert, H., and Wendisch, M.: Case study of a humidity  
1061 layer above Arctic stratocumulus and potential turbulent coupling with the cloud top, *Atmospheric Chemistry and Physics*,  
1062 21, 6347–6364, <https://doi.org/10.5194/acp-21-6347-2021>, 2021.

1063 Egerer, U., Siebert, H., Hellmuth, O., and Sørensen, L. L.: The role of a low-level jet for stirring the stable atmospheric surface  
1064 layer in the Arctic, *Atmospheric Chemistry and Physics*, 23, 15365–15373, <https://doi.org/10.5194/acp-23-15365-2023>, 2023.

1065 Engel, A.: Distribution of transparent exopolymer particles (TEP) in the northeast Atlantic Ocean and their potential  
1066 significance for aggregation processes, *Deep Sea Research Part I: Oceanographic Research Papers*, 51, 83–92,  
1067 <https://doi.org/10.1016/j.dsr.2003.09.001>, 2004.

1068 Engel, A. and Galgani, L.: The organic sea-surface microlayer in the upwelling region off the coast of Peru and potential  
1069 implications for air–sea exchange processes, *Biogeosciences (BG)*, 13, 989–1007, <https://doi.org/10.5194/bg-13-989-2016>,  
1070 2016.

1071 Engel, A. and Händel, N.: A novel protocol for determining the concentration and composition of sugars in particulate and in  
1072 high molecular weight dissolved organic matter (HMW-DOM) in seawater, *Marine Chemistry*, 127, 180–191,  
1073 <https://doi.org/10.1016/j.marchem.2011.09.004>, 2011.

1074 Engel, A., Thoms, S., Riebesell, U., Rochelle-Newall, E., and Zondervan, I.: Polysaccharide aggregation as a potential sink of  
1075 marine dissolved organic carbon, *Nature*, 428, 929–932, <https://doi.org/10.1038/nature02453>, 2004.

1076 Engel, A., Harlay, J., Piontek, J., and Chou, L.: Contribution of combined carbohydrates to dissolved and particulate organic  
1077 carbon after the spring bloom in the northern Bay of Biscay (North-Eastern Atlantic Ocean), *Continental Shelf Research*, 45,  
1078 42–53, <https://doi.org/10.1016/j.csr.2012.05.016>, 2012.

1079 Ervens, B. and Amato, P.: The global impact of bacterial processes on carbon mass, *Atmospheric Chemistry & Physics*, 20,  
1080 1777–1794, <https://doi.org/10.5194/acp-20-1777-2020>, 2020.

1081 Esau, I. and Repina, I.: Wind Climate in Kongsfjorden, Svalbard, and Attribution of Leading Wind Driving Mechanisms through  
1082 Turbulence-Resolving Simulations, *Advances in Meteorology*, 2012, 568454, <https://doi.org/10.1155/2012/568454>, 2012.

1083 Fabiano, M., Povero, P., and Danovaro, R.: Distribution and composition of particulate organic matter in the Ross Sea  
1084 (Antarctica), *Polar Biol*, 13, 525–533, <https://doi.org/10.1007/BF00236394>, 1993.

1085 Facchini, M. C., Rinaldi, M., Decesari, S., Carbone, C., Finessi, E., Mircea, M., Fuzzi, S., Ceburnis, D., Flanagan, R., Nilsson, E. D.,  
1086 Leeuw, G. de, Martino, M., Woeltjen, J., and O’Dowd, C. D.: Primary submicron marine aerosol dominated by insoluble organic  
1087 colloids and aggregates, *Geophysical Research Letters*, 35, 1–5, <https://doi.org/10.1029/2008GL034210>, 2008.

1088 Farmer, D. K., Cappa, C. D., and Kreidenweis, S. M.: Atmospheric Processes and Their Controlling Influence on Cloud  
1089 Condensation Nuclei Activity, *Chem. Rev.*, 115, 4199–4217, <https://doi.org/10.1021/cr5006292>, 2015.

1090 Farmer, D. K., Boedicker, E. K., and DeBolt, H. M.: Dry Deposition of Atmospheric Aerosols: Approaches, Observations, and  
1091 Mechanisms, *Annual Review of Physical Chemistry*, 72, 375–397, <https://doi.org/10.1146/annurev-physchem-090519-034936>, 2021.

1093 Feltracco, M., Barbaro, E., Hoppe, C. J. M., Wolf, K. K. E., Spolaor, A., Layton, R., Keuschnig, C., Barbante, C., Gambaro, A., and  
1094 Larose, C.: Airborne bacteria and particulate chemistry capture Phytoplankton bloom dynamics in an Arctic fjord, *Atmospheric  
1095 Environment*, 256, 118458, <https://doi.org/10.1016/j.atmosenv.2021.118458>, 2021.

1096 Fomba, K. W., Müller, K., van Pinxteren, D., Poulain, L., van Pinxteren, M., and Herrmann, H.: Long-term chemical  
1097 characterization of tropical and marine aerosols at the Cape Verde Atmospheric Observatory (CVAO) from 2007 to 2011,  
1098 *Atmospheric Chemistry and Physics*, 14, 8883–8904, <https://doi.org/10.5194/acp-14-8883-2014>, 2014.

1099 Francis, J. A. and Wu, B.: Why has no new record-minimum Arctic sea-ice extent occurred since September 2012?, *Environ.  
1100 Res. Lett.*, 15, 114034, <https://doi.org/10.1088/1748-9326/abc047>, 2020.

1101 Freud, E., Krejci, R., Tunved, P., Leaitch, R., Nguyen, Q. T., Massling, A., Skov, H., and Barrie, L.: Pan-Arctic aerosol number size  
1102 distributions: seasonality and transport patterns, *Atmospheric Chemistry and Physics*, 17, 8101–8128,  
1103 <https://doi.org/10.5194/acp-17-8101-2017>, 2017.

1104 Furukawa, T. and Takahashi, Y.: Oxalate metal complexes in aerosol particles: implications for the hygroscopicity of oxalate-  
1105 containing particles, *Atmos. Chem. Phys.*, 11, 4289–4301, <https://doi.org/10.5194/acp-11-4289-2011>, 2011.

1106 Gantt, B., Meskhidze, N., Facchini, M. C., Rinaldi, M., Ceburnis, D., and O’Dowd, C. D.: Wind speed dependent size-resolved  
1107 parameterization for the organic mass fraction of sea spray aerosol, *Atmospheric Chemistry and Physics*, 11, 8777–8790,  
1108 <https://doi.org/10.5194/acp-11-8777-2011>, 2011.

1109 Gao, Q., Leck, C., Rauschenberg, C., and Matrai, P. A.: On the chemical dynamics of extracellular polysaccharides in the high  
1110 Arctic surface microlayer, *Ocean Science*, 8, 401–418, <https://doi.org/10.5194/os-8-401-2012>, 2012.

1111 Gierens, R., Kneifel, S., Shupe, M. D., Ebell, K., Maturilli, M., and Löhnert, U.: Low-level mixed-phase clouds in a complex Arctic  
1112 environment, *Atmospheric Chemistry and Physics*, 20, 3459–3481, <https://doi.org/10.5194/acp-20-3459-2020>, 2020.

1113 Goldberg, S. J., Carlson, C. A., Brzezinski, M., Nelson, N. B., and Siegel, D. A.: Systematic removal of neutral sugars within  
1114 dissolved organic matter across ocean basins, *Geophysical Research Letters*, 38, 1–7,  
1115 <https://doi.org/10.1029/2011GL048620>, 2011.

1116 Grawe, S., Jentsch, C., Schaefer, J., Wex, H., Mertes, S., and Stratmann, F.: Next-generation ice-nucleating particle sampling  
1117 on board aircraft: characterization of the High-volume flow aERosol particle filter sAmplifier (HERA), *Atmospheric Measurement  
1118 Techniques*, 16, 4551–4570, <https://doi.org/10.5194/amt-16-4551-2023>, 2023.

1119 Grolemond, G. and Wickham, H.: Dates and Times Made Easy with lubridate, *Journal of Statistical Software*, 40, 1–25, 2011.

1120 Grosse, J., Nöthig, E.-M., Torres-Valdés, S., and Engel, A.: Summertime Amino Acid and Carbohydrate Patterns in Particulate  
1121 and Dissolved Organic Carbon Across Fram Strait, *Front. Mar. Sci.*, 8, <https://doi.org/10.3389/fmars.2021.684675>, 2021.

1122 Guo, T., Li, K., Zhu, Y., Gao, H., and Yao, X.: Concentration and size distribution of particulate oxalate in marine and coastal  
1123 atmospheres – Implication for the increased importance of oxalate in nanometer atmospheric particles, *Atmospheric  
1124 Environment*, 142, 19–31, <https://doi.org/10.1016/j.atmosenv.2016.07.026>, 2016.

1125 Gürses, Ö., Oziel, L., Karakuş, O., Sidorenko, D., Völker, C., Ye, Y., Zeising, M., Butzin, M., and Hauck, J.: Ocean biogeochemistry  
1126 in the coupled ocean–sea ice–biogeochemistry model FESOM2.1–REcoM3, *Geoscientific Model Development*, 16, 4883–  
1127 4936, <https://doi.org/10.5194/gmd-16-4883-2023>, 2023.

1128 Haddrell, A. E. and Thomas, R. J.: Aerobiology: Experimental Considerations, Observations, and Future Tools, *Appl. Environ.  
1129 Microbiol.*, 83, 1–15, <https://doi.org/10.1128/AEM.00809-17>, 2017.

1130 Hansell, D. A.: Recalcitrant Dissolved Organic Carbon Fractions, *Annual Review of Marine Science*, 5, 421–445,  
1131 <https://doi.org/10.1146/annurev-marine-120710-100757>, 2013.

1132 Hara, K., Yamagata, S., Yamanouchi, T., Sato, K., Herber, A., Iwasaka, Y., Nagatani, M., and Nakata, H.: Mixing states of  
1133 individual aerosol particles in spring Arctic troposphere during ASTAR 2000 campaign, *Journal of Geophysical Research:  
1134 Atmospheres*, 108, 1–12, <https://doi.org/10.1029/2002JD002513>, 2003.

1135 Hartmann, S., Schrödner, R., Hassett, B. T., Hartmann, M., van Pinxteren, M., Fomba, K. W., Stratmann, F., Herrmann, H.,  
1136 Pöhler, M., and Zeppenfeld, S.: Polysaccharides—Important Constituents of Ice-Nucleating Particles of Marine Origin,  
1137 *Environ. Sci. Technol.*, 59, 5098–5108, <https://doi.org/10.1021/acs.est.4c08014>, 2025.

1138 Hasenecz, E., Jayarathne, T., Pendergraft, M. A., Santander, M. V., Mayer, K. J., Sauer, J., Lee, C., Gibson, W. S., Kruse, S. M.,  
1139 Malfatti, F., Prather, K. A., and Stone, E. A.: Marine bacteria affect saccharide enrichment in sea spray aerosol during a  
1140 phytoplankton bloom, *ACS Earth Space Chem.*, 4, 1638–1649, <https://doi.org/10.1021/acsearthspacechem.0c00167>, 2020.

1141 Hasenecz, E. S., Kaluarachchi, C. P., Lee, H. D., Tivanski, A. V., and Stone, E. A.: Saccharide Transfer to Sea Spray Aerosol  
1142 Enhanced by Surface Activity, Calcium, and Protein Interactions, *ACS Earth Space Chem.*, 3, 2539–2548,  
1143 <https://doi.org/10.1021/acsearthspacechem.9b00197>, 2019.

1144 Herrmann, H., Tilgner, A., Barzaghi, P., Majdik, Z., Gligorovski, S., Poulain, L., and Monod, A.: Towards a more detailed  
1145 description of tropospheric aqueous phase organic chemistry: CAPRAM 3.0, *Atmospheric Environment*, 39, 4351–4363,  
1146 <https://doi.org/10.1016/j.atmosenv.2005.02.016>, 2005.

1147 Heutte, B., Bergner, N., Angot, H., Pernov, J. B., Dada, L., Mirrielees, J. A., Beck, I., Baccarini, A., Boyer, M., Creamean, J. M.,  
1148 Daellenbach, K. R., El Haddad, I., Frey, M. M., Henning, S., Laurila, T., Moschos, V., Petäjä, T., Pratt, K. A., Quéléver, L. L. J.,  
1149 Shupe, M. D., Zieger, P., Jokinen, T., and Schmale, J.: Observations of high-time-resolution and size-resolved aerosol chemical  
1150 composition and microphysics in the central Arctic: implications for climate-relevant particle properties, *Atmospheric  
1151 Chemistry and Physics*, 25, 2207–2241, <https://doi.org/10.5194/acp-25-2207-2025>, 2025.

1152 Hijmans, R. J.: raster: Geographic Data Analysis and Modeling, R package version 3.6-26, 2023.

1153 Hill, T. C. J., Malfatti, F., McCluskey, C. S., Schill, G. P., Santander, M. V., Moore, K. A., Rauker, A. M., Perkins, R. J., Celussi, M.,  
1154 Levin, E. J. T., Suski, K. J., Cornwell, G. C., Lee, C., Negro, P. D., Kreidenweis, S. M., Prather, K. A., and DeMott, P. J.: Resolving  
1155 the controls over the production and emission of ice-nucleating particles in sea spray, *Environ. Sci.: Atmos.*,  
1156 <https://doi.org/10.1039/D2EA00154C>, 2023.

1157 Hoffman, E. J. and Duce, R. A.: Factors influencing the organic carbon content of marine aerosols: A laboratory study, *Journal  
1158 of Geophysical Research (1896-1977)*, 81, 3667–3670, <https://doi.org/10.1029/JC081i021p03667>, 1976.

1159 Hogan, R. J., Mittermaier, M. P., and Illingworth, A. J.: The Retrieval of Ice Water Content from Radar Reflectivity Factor and  
1160 Temperature and Its Use in Evaluating a Mesoscale Model, *Journal of Applied Meteorology and Climatology*, 45, 301–317,  
1161 <https://doi.org/10.1175/JAM2340.1>, 2006.

1162 Hoppel, W. A., Frick, G. M., and Fitzgerald, J. W.: Surface source function for sea-salt aerosol and aerosol dry deposition to  
1163 the ocean surface, *Journal of Geophysical Research: Atmospheres*, 107, AAC 7-1-AAC 7-17,  
1164 <https://doi.org/10.1029/2001JD002014>, 2002.

1165 Illingworth, A. J., Hogan, R. J., O'Connor, E. J., Bouniol, D., Brooks, M. E., Delanoé, J., Donovan, D. P., Eastment, J. D., Gaussiat,  
1166 N., Goddard, J. W. F., Haeffelin, M., Baltink, H. K., Krasnov, O. A., Pelon, J., Piriou, J.-M., Protat, A., Russchenberg, H. W. J.,  
1167 Seifert, A., Tompkins, A. M., Zadelhoff, G.-J. van, Vinit, F., Willén, U., Wilson, D. R., and Wrench, C. L.: Cloudnet: Continuous

1168 Evaluation of Cloud Profiles in Seven Operational Models Using Ground-Based Observations, *Bulletin of the American*  
1169 *Meteorological Society*, 88, 883–898, <https://doi.org/10.1175/BAMS-88-6-883>, 2007.

1170 Ittekkot, V., Brockmann, U., Michaelis, W., and Degens, E. T.: Dissolved free and combined carbohydrates during a  
1171 phytoplankton bloom in the northern North Sea, *Marine Ecology Progress Series*, 4, 299–305, 1981.

1172 Jayarathne, T., Sultana, C. M., Lee, C., Malfatti, F., Cox, J. L., Pendergraft, M. A., Moore, K. A., Azam, F., Tivanski, A. V., Cappa,  
1173 C. D., Bertram, T. H., Grassian, V. H., Prather, K. A., and Stone, E. A.: Enrichment of Saccharides and Divalent Cations in Sea  
1174 Spray Aerosol During Two Phytoplankton Blooms, *Environ Sci Technol*, 50, 11511–11520,  
1175 <https://doi.org/10.1021/acs.est.6b02988>, 2016.

1176 Jensen, L. Z., Glasius, M., Gryning, S.-E., Massling, A., Finster, K., and Šantl-Temkiv, T.: Seasonal Variation of the Atmospheric  
1177 Bacterial Community in the Greenlandic High Arctic Is Influenced by Weather Events and Local and Distant Sources, *Front.*  
1178 *Microbiol.*, 13, <https://doi.org/10.3389/fmicb.2022.909980>, 2022.

1179 Kang, H., Jung, C. H., Lee, B. Y., Krejci, R., Heslin-Rees, D., Aas, W., and Yoon, Y. J.: Aerosol hygroscopicity influenced by  
1180 seasonal chemical composition variations in the Arctic region, *Journal of Aerosol Science*, 106551,  
1181 <https://doi.org/10.1016/j.jaerosci.2025.106551>, 2025.

1182 Kanji, Z. A., Ladino, L. A., Wex, H., Boose, Y., Burkert-Kohn, M., Cziczo, D. J., and Krämer, M.: Overview of Ice Nucleating  
1183 Particles, *Meteorological Monographs*, 58, 1.1-1.33, <https://doi.org/10.1175/AMSMONOGRAPH5-D-16-0006.1>, 2017.

1184 Karl, M., Leck, C., Rad, F. M., Bäcklund, A., Lopez-Aparicio, S., and Heintzenberg, J.: New insights in sources of the sub-  
1185 micrometre aerosol at Mt. Zeppelin observatory (Spitsbergen) in the year 2015, *Tellus B: Chemical and Physical Meteorology*,  
1186 71, 1613143, <https://doi.org/10.1080/16000889.2019.1613143>, 2019.

1187 Kawamura, K. and Bikkina, S.: A review of dicarboxylic acids and related compounds in atmospheric aerosols: Molecular  
1188 distributions, sources and transformation, *Atmospheric Research*, 170, 140–160,  
1189 <https://doi.org/10.1016/j.atmosres.2015.11.018>, 2016.

1190 Kawamura, K., Kasukabe, H., and Barrie, L. A.: Source and reaction pathways of dicarboxylic acids, ketoacids and dicarbonyls  
1191 in arctic aerosols: One year of observations, *Atmospheric Environment*, 30, 1709–1722, [https://doi.org/10.1016/1352-2310\(95\)00395-9](https://doi.org/10.1016/1352-2310(95)00395-9), 1996a.

1193 Kawamura, K., Sempéré, R., Imai, Y., Fujii, Y., and Hayashi, M.: Water soluble dicarboxylic acids and related compounds in  
1194 Antarctic aerosols, *Journal of Geophysical Research: Atmospheres*, 101, 18721–18728, <https://doi.org/10.1029/96JD01541>,  
1195 1996b.

1196 Keene, W. C., Pszenny, A. A. P., Galloway, J. N., and Hawley, M. E.: Sea-salt corrections and interpretation of constituent ratios  
1197 in marine precipitation, *Journal of Geophysical Research*, 91, 6647–6658, <https://doi.org/10.1029/JD091iD06p06647>, 1986.

1198 Keene, W. C., Long, M. S., Reid, J. S., Frossard, A. A., Kieber, D. J., Maben, J. R., Russell, L. M., Kinsey, J. D., Quinn, P. K., and  
1199 Bates, T. S.: Factors That Modulate Properties of Primary Marine Aerosol Generated From Ambient Seawater on Ships at Sea,  
1200 *Journal of Geophysical Research: Atmospheres*, 122, 11,961-11,990, <https://doi.org/10.1002/2017JD026872>, 2017.

1201 Kerminen, V.-M., Teinilä, K., Hillamo, R., and Mäkelä, T.: Size-segregated chemistry of particulate dicarboxylic acids in the  
1202 Arctic atmosphere, *Atmospheric Environment*, 33, 2089–2100, [https://doi.org/10.1016/S1352-2310\(98\)00350-1](https://doi.org/10.1016/S1352-2310(98)00350-1), 1999.

1203 Khadem, H. E.: *Carbohydrate Chemistry: Monosaccharides and Their Oligomers*, Elsevier, 267 pp., 2012.

1204 Kharbush, J. J., Close, H. G., Van Mooy, B. A. S., Arnosti, C., Smittenberg, R. H., Le Moigne, F. A. C., Mollenhauer, G., Scholz-  
1205 Böttcher, B., Obrecht, I., Koch, B. P., Becker, K., Iversen, M. H., and Mohr, W.: Particulate Organic Carbon Deconstructed:  
1206 Molecular and Chemical Composition of Particulate Organic Carbon in the Ocean, *Frontiers in Marine Science*, 7, Art.Nr. 518,  
1207 <https://doi.org/10.3389/fmars.2020.00518>, 2020.

1208 Kirchman, D. L., Meon, B., Ducklow, H. W., Carlson, C. A., Hansell, D. A., and Steward, G. F.: Glucose fluxes and concentrations  
1209 of dissolved combined neutral sugars (polysaccharides) in the Ross Sea and Polar Front Zone, Antarctica, *Deep Sea Research*  
1210 *Part II: Topical Studies in Oceanography*, 48, 4179–4197, [https://doi.org/10.1016/S0967-0645\(01\)00085-6](https://doi.org/10.1016/S0967-0645(01)00085-6), 2001.

1211 Klein, A. M., Bohannon, B. J. M., Jaffe, D. A., Levin, D. A., and Green, J. L.: Molecular Evidence for Metabolically Active Bacteria  
1212 in the Atmosphere, *Front. Microbiol.*, 7, 772, <https://doi.org/10.3389/fmicb.2016.00772>, 2016.

1213 Köllner, F., Schneider, J., Willis, M. D., Klimach, T., Helleis, F., Bozem, H., Kunkel, D., Hoor, P., Burkart, J., Leaitch, W. R.,  
1214 Aliabadi, A. A., Abbatt, J. P. D., Herber, A. B., and Borrmann, S.: Particulate trimethylamine in the summertime Canadian high  
1215 Arctic lower troposphere, *Atmospheric Chemistry and Physics*, 17, 13747–13766, [https://doi.org/10.5194/acp-17-13747-](https://doi.org/10.5194/acp-17-13747-2017)  
1216 2017, 2017.

1217 Leck, C., Gao, Q., Mashayekhy Rad, F., and Nilsson, U.: Size-resolved atmospheric particulate polysaccharides in the high  
1218 summer Arctic, *Atmospheric Chemistry and Physics*, 13, 12573–12588, <https://doi.org/10.5194/acp-13-12573-2013>, 2013.

1219 Leon-Marcos, A., Zeising, M., van Pinxteren, M., Zeppenfeld, S., Bracher, A., Barbaro, E., Engel, A., Feltracco, M., Tegen, I., and  
1220 Heinold, B.: Modelling emission and transport of key components of primary marine organic aerosol using the global aerosol-  
1221 climate model ECHAM6.3–HAM2.3, *Geoscientific Model Development*, 18, 4183–4213, [https://doi.org/10.5194/gmd-18-](https://doi.org/10.5194/gmd-18-4183-2025)  
1222 4183-2025, 2025.

- 1223 Li, J., Han, Z., Fu, P., Yao, X., and Liang, M.: Seasonal characteristics of emission, distribution, and radiative effect of marine  
1224 organic aerosols over the western Pacific Ocean: an investigation with a coupled regional climate aerosol model, *Atmospheric*  
1225 *Chemistry and Physics*, 24, 3129–3161, <https://doi.org/10.5194/acp-24-3129-2024>, 2024.
- 1226 Lohmann, U. and Feichter, J.: Global indirect aerosol effects: a review, *Atmospheric Chemistry and Physics*, 5, 715–737,  
1227 <https://doi.org/10.5194/acp-5-715-2005>, 2005.
- 1228 **Macke, A. and Flores, H.: The Expeditions PS106/1 and 2 of the Research Vessel POLARSTERN to the Arctic Ocean in 2017,**  
1229 **Bremerhaven, Germany, 171 pp., [https://doi.org/10.2312/BzPM\\_0719\\_2018\\_2018](https://doi.org/10.2312/BzPM_0719_2018_2018).**
- 1230 Madry, W. L., Toon, O. B., and O’Dowd, C. D.: Modeled optical thickness of sea-salt aerosol, *Journal of Geophysical Research: Atmospheres*, 116, <https://doi.org/10.1029/2010JD014691>, 2011.
- 1232 Malfatti, F., Lee, C., Tinta, T., Pendergraft, M. A., Celussi, M., Zhou, Y., Sultana, C. M., Rotter, A., Axson, J. L., Collins, D. B.,  
1233 Santander, M. V., Anides Morales, A. L., Aluwihare, L. I., Riemer, N., Grassian, V. H., Azam, F., and Prather, K. A.: Detection of  
1234 Active Microbial Enzymes in Nascent Sea Spray Aerosol: Implications for Atmospheric Chemistry and Climate, *Environ. Sci.*  
1235 *Technol. Lett.*, 6, 171–177, <https://doi.org/10.1021/acs.estlett.8b00699>, 2019.
- 1236 Manders, A. M. M., Schaap, M., Querol, X., Albert, M. F. M. A., Vercauteren, J., Kuhlbusch, T. A. J., and Hoogerbrugge, R.: Sea  
1237 salt concentrations across the European continent, *Atmospheric Environment*, 44, 2434–2442,  
1238 <https://doi.org/10.1016/j.atmosenv.2010.03.028>, 2010.
- 1239 Matulová, M., Husárová, S., Capek, P., Sancelme, M., and Delort, A.-M.: Biotransformation of Various Saccharides and  
1240 Production of Exopolymeric Substances by Cloud-Borne Bacillus sp. 3B6, *Environ. Sci. Technol.*, 48, 14238–14247,  
1241 <https://doi.org/10.1021/es501350s>, 2014.
- 1242 Maturilli, M.: Continuous meteorological observations at station Ny-Ålesund (2011-08 et seq), Alfred Wegener Institute -  
1243 Research Unit Potsdam, <https://doi.org/10.1594/PANGAEA.914979>, 2020.
- 1244 Maturilli, M., Herber, A., and König-Langlo, G.: Climatology and time series of surface meteorology in Ny-Ålesund, Svalbard,  
1245 *Earth System Science Data*, 5, 155–163, <https://doi.org/10.5194/essd-5-155-2013>, 2013.
- 1246 Maturilli, M., Herber, A., and König-Langlo, G.: Surface radiation climatology for Ny-Ålesund, Svalbard (78.9° N), basic  
1247 observations for trend detection, *Theor Appl Climatol*, 120, 331–339, <https://doi.org/10.1007/s00704-014-1173-4>, 2015.
- 1248 Mayot, N., Matrai, P., Ellingsen, I. H., Steele, M., Johnson, K., Riser, S. C., and Swift, D.: Assessing Phytoplankton Activities in  
1249 the Seasonal Ice Zone of the Greenland Sea Over an Annual Cycle, *Journal of Geophysical Research: Oceans*, 123, 8004–8025,  
1250 <https://doi.org/10.1029/2018JC014271>, 2018.
- 1251 McNeill, V. F.: Aqueous Organic Chemistry in the Atmosphere: Sources and Chemical Processing of Organic Aerosols, *Environ.*  
1252 *Technol.*, 49, 1237–1244, <https://doi.org/10.1021/es5043707>, 2015.
- 1253 Mirrielees, J. A., Kirpes, R. M., Costa, E. J., Porter, G. C. E., Murray, B. J., Lata, N. N., Boschi, V., China, S., Grannas, A. M., Ault,  
1254 A. P., Matrai, P. A., and Pratt, K. A.: Marine aerosol generation experiments in the High Arctic during summertime, *Elementa:*  
1255 *Science of the Anthropocene*, 12, 00134, <https://doi.org/10.1525/elementa.2023.00134>, 2024.
- 1256 Müller, K., Lehmann, S., Pinxteren, D. van, Gnauk, T., Niedermeier, N., Wiedensohler, A., and Herrmann, H.: Particle  
1257 characterization at the Cape Verde atmospheric observatory during the 2007 RHaMBLE intensive, *Atmospheric Chemistry*  
1258 *and Physics*, 10, 2709–2721, <https://doi.org/10.5194/acp-10-2709-2010>, 2010.
- 1259 Neuwirth, E.: RColorBrewer: ColorBrewer Palettes, R package version 1.1-3, 2022.
- 1260 Nomokonova, T., Ebell, K., Löhnert, U., Maturilli, M., Ritter, C., and O’Connor, E.: Statistics on clouds and their relation to  
1261 thermodynamic conditions at Ny-Ålesund using ground-based sensor synergy, *Atmospheric Chemistry and Physics*, 19, 4105–  
1262 4126, <https://doi.org/10.5194/acp-19-4105-2019>, 2019.
- 1263 O’Dowd, C. D. and de Leeuw, G.: Marine aerosol production: a review of the current knowledge, *Philos Trans A Math Phys*  
1264 *Eng Sci*, 365, 1753–1774, <https://doi.org/10.1098/rsta.2007.2043>, 2007.
- 1265 O’Dowd, C. D., Smith, M. H., Consterdine, I. E., and Lowe, J. A.: Marine aerosol, sea-salt, and the marine sulphur cycle: a short  
1266 review, *Atmospheric Environment*, 31, 73–80, [https://doi.org/10.1016/S1352-2310\(96\)00106-9](https://doi.org/10.1016/S1352-2310(96)00106-9), 1997.
- 1267 Ooki, A., Uematsu, M., Miura, K., and Nakae, S.: Sources of sodium in atmospheric fine particles, *Atmospheric Environment*,  
1268 36, 4367–4374, [https://doi.org/10.1016/S1352-2310\(02\)00341-2](https://doi.org/10.1016/S1352-2310(02)00341-2), 2002.
- 1269 Orellana, M. V. and Leck, C.: Chapter 9 - Marine Microgels, in: *Biogeochemistry of Marine Dissolved Organic Matter (Second*  
1270 *Edition)*, edited by: Hansell, D. A. and Carlson, C. A., Academic Press, Boston, 451–480, <https://doi.org/10.1016/B978-0-12-405940-5.00009-1>, 2015.
- 1272 Orellana, M. V., Matrai, P. A., Leck, C., Rauschenberg, C. D., Lee, A. M., and Coz, E.: Marine microgels as a source of cloud  
1273 condensation nuclei in the high Arctic, *PNAS*, 108, 13612–13617, <https://doi.org/10.1073/pnas.1102457108>, 2011.
- 1274 Oziel, L., Schourup-Kristensen, V., Wekerle, C., and Hauck, J.: The Pan-Arctic Continental Slope as an Intensifying Conveyor  
1275 Belt for Nutrients in the Central Arctic Ocean (1985–2015), *Global Biogeochemical Cycles*, 36, e2021GB007268,  
1276 <https://doi.org/10.1029/2021GB007268>, 2022.

Formatiert: Abstand Nach: 6 Pt.

1277 Panagiotopoulos, C. and Sempéré, R.: Analytical methods for the determination of sugars in marine samples: A historical  
1278 perspective and future directions, *Limnology and Oceanography: Methods*, 3, 419–454,  
1279 <https://doi.org/10.4319/lom.2005.3.419>, 2005.

1280 Penner, J. E., Andreae, M. O., Annegarn, H., Barrie, L., Feichter, J., Hegg, D., Jayaraman, A., Leaitch, R., Murphy, D., Nganga,  
1281 J., and Pitari, G.: Aerosols, their Direct and Indirect Effects, *Climate Change 2001: The Scientific Basis. Contribution of Working  
1282 Group I to the Third Assessment Report of the Intergovernmental Panel on Climate Change*, 289–348, 2001.

1283 Pierce, D.: ncd4: Interface to Unidata netCDF (Version 4 or Earlier) Format Data, R package version 1.22, 2023.

1284 Pilinis, C., Pandis, S. N., and Seinfeld, J. H.: Sensitivity of direct climate forcing by atmospheric aerosols to aerosol size and  
1285 composition, *Journal of Geophysical Research*, 100, 18,739–18,754, <https://doi.org/10.1029/95JD02119>, 1995.

1286 Pilz, C., Düsing, S., Wehner, B., Müller, T., Siebert, H., Voigtländer, J., and Lonardi, M.: CAMP: an instrumented platform for  
1287 balloon-borne aerosol particle studies in the lower atmosphere, *Atmospheric Measurement Techniques*, 15, 6889–6905,  
1288 <https://doi.org/10.5194/amt-15-6889-2022>, 2022.

1289 Pilz, C., Lonardi, M., Egerer, U., Siebert, H., Ehrlich, A., Heymsfield, A. J., Schmitt, C. G., Shupe, M. D., Wehner, B., and  
1290 Wendisch, M.: Profile observations of the Arctic atmospheric boundary layer with the BELUGA tethered balloon during  
1291 MOSAiC, *Sci Data*, 10, 534, <https://doi.org/10.1038/s41597-023-02423-5>, 2023.

1292 Pilz, C., Cassano, J. J., de Boer, G., Kirbus, B., Lonardi, M., Pöhlker, M., Shupe, M. D., Siebert, H., Wendisch, M., and Wehner,  
1293 B.: Tethered balloon measurements reveal enhanced aerosol occurrence aloft interacting with Arctic low-level clouds,  
1294 *Elementa: Science of the Anthropocene*, 12, 00120, <https://doi.org/10.1525/elementa.2023.00120>, 2024.

1295 van Pinxteren, M., Müller, C., Iinuma, Y., Stolle, C., and Herrmann, H.: Chemical Characterization of Dissolved Organic  
1296 Compounds from Coastal Sea Surface Microlayers (Baltic Sea, Germany), *Environmental Science & Technology*, 46, 10455–  
1297 10462, <https://doi.org/10.1021/es204492b>, 2012.

1298 van Pinxteren, M., Barthel, S., Fomba, K. W., Müller, K., Von Tümpling, W., and Herrmann, H.: The influence of environmental  
1299 drivers on the enrichment of organic carbon in the sea surface microlayer and in submicron aerosol particles – measurements  
1300 from the Atlantic Ocean, *Elem Sci Anth*, 5, 1–21, <https://doi.org/10.1525/elementa.225>, 2017.

1301 van Pinxteren, M., Robinson, T.-B., Zeppenfeld, S., Gong, X., Bahlmann, E., Fomba, K. W., Triesch, N., Stratmann, F., Wurl, O.,  
1302 Engel, A., Wex, H., and Herrmann, H.: High number concentrations of transparent exopolymer particles in ambient aerosol  
1303 particles and cloud water – a case study at the tropical Atlantic Ocean, *Atmospheric Chemistry and Physics*, 22, 5725–5742,  
1304 <https://doi.org/10.5194/acp-22-5725-2022>, 2022.

1305 van Pinxteren, M., Zeppenfeld, S., Fomba, K. W., Triesch, N., Frka, S., and Herrmann, H.: Amino acids, carbohydrates, and  
1306 lipids in the tropical oligotrophic Atlantic Ocean: sea-to-air transfer and atmospheric in situ formation, *Atmospheric Chemistry  
1307 and Physics*, 23, 6571–6590, <https://doi.org/10.5194/acp-23-6571-2023>, 2023.

1308 Platt, S. M., Hov, Ø., Berg, T., Breivik, K., Eckhardt, S., Eleftheriadis, K., Evangeliou, N., Fiebig, M., Fisher, R., Hansen, G.,  
1309 Hansson, H.-C., Heintzenberg, J., Hermansen, O., Heslin-Rees, D., Holmén, K., Hudson, S., Kallenborn, R., Krejci, R., Krognæs,  
1310 T., Larssen, S., Lowry, D., Lund Myhre, C., Lunder, C., Nisbet, E., Nizzetto, P. B., Park, K.-T., Pedersen, C. A., Aspö Pfaffhuber,  
1311 K., Röckmann, T., Schmidbauer, N., Solberg, S., Stohl, A., Ström, J., Svendby, T., Tunved, P., Tørnkvist, K., van der Veen, C.,  
1312 Vratolis, S., Yoon, Y. J., Yttri, K. E., Zieger, P., Aas, W., and Tørseth, K.: Atmospheric composition in the European Arctic and  
1313 30 years of the Zeppelin Observatory, Ny-Ålesund, *Atmospheric Chemistry and Physics*, 22, 3321–3369,  
1314 <https://doi.org/10.5194/acp-22-3321-2022>, 2022.

1315 van de Poll, W. H., Maat, D. S., Fischer, P., Visser, R. J. W., Brussaard, C. P. D., and Buma, A. G. J.: Solar radiation and solar  
1316 radiation driven cycles in warming and freshwater discharge control seasonal and inter-annual phytoplankton chlorophyll a  
1317 and taxonomic composition in a high Arctic fjord (Kongsfjorden, Spitsbergen), *Limnology and Oceanography*, 66, 1221–1236,  
1318 <https://doi.org/10.1002/lno.11677>, 2021.

1319 Porter, G. C. E., Adams, M. P., Brooks, I. M., Ickes, L., Karlsson, L., Leck, C., Salter, M. E., Schmale, J., Siegel, K., Sikora, S. N. F.,  
1320 Tarn, M. D., Vüllers, J., Wernli, H., Zieger, P., Zinke, J., and Murray, B. J.: Highly Active Ice-Nucleating Particles at the Summer  
1321 North Pole, *Journal of Geophysical Research: Atmospheres*, 127, e2021JD036059, <https://doi.org/10.1029/2021JD036059>,  
1322 2022.

1323 Quinn, P. K., Collins, D. B., Grassian, V. H., Prather, K. A., and Bates, T. S.: Chemistry and Related Properties of Freshly Emitted  
1324 Sea Spray Aerosol, *Chemical Reviews*, 115, 4383–4399, <https://doi.org/10.1021/cr500713g>, 2015.

1325 Ramasamy, K. P., Mahawar, L., Rajasabapathy, R., Rajeshwari, K., Miceli, C., and Pucciarelli, S.: Comprehensive insights on  
1326 environmental adaptation strategies in Antarctic bacteria and biotechnological applications of cold adapted molecules, *Front.  
1327 Microbiol.*, 14, <https://doi.org/10.3389/fmicb.2023.1197797>, 2023.

1328 Rinaldi, M., Decesari, S., Carbone, C., Finessi, E., Fuzzi, S., Ceburnis, D., O'Dowd, C. D., Sciare, J., Burrows, J. P., Vrekoussis, M.,  
1329 Ervens, B., Tsigaridis, K., and Facchini, M. C.: Evidence of a natural marine source of oxalic acid and a possible link to glyoxal,  
1330 *Journal of Geophysical Research: Atmospheres*, 116, <https://doi.org/10.1029/2011JD015659>, 2011.

1331 Robinson, T.-B., Stolle, C., and Wurl, O.: Depth is relative: the importance of depth for transparent exopolymer particles in  
1332 the near-surface environment, *Ocean Science*, 15, 1653–1666, <https://doi.org/10.5194/os-15-1653-2019>, 2019a.

- 1333 Robinson, T.-B., Wurl, O., Bahlmann, E., Jürgens, K., and Stolle, C.: Rising bubbles enhance the gelatinous nature of the air–  
1334 sea interface, *Limnology and Oceanography*, 64, 2358–2372, <https://doi.org/10.1002/lno.11188>, 2019b.
- 1335 Rocchi, A., von Jackowski, A., Welti, A., Li, G., Kanji, Z. A., Povazhnyy, V., Engel, A., Schmale, J., Nenes, A., Berdalet, E., Simó,  
1336 R., and Dall'Osto, M.: Glucose Enhances Salinity-Driven Sea Spray Aerosol Production in Eastern Arctic Waters, *Environ. Sci.*  
1337 *Technol.*, 58, 8748–8759, <https://doi.org/10.1021/acs.est.4c02826>, 2024.
- 1338 Russell, L. M., Hawkins, L. N., Frossard, A. A., Quinn, P. K., and Bates, T. S.: Carbohydrate-like composition of submicron  
1339 atmospheric particles and their production from ocean bubble bursting, *Proc. Natl. Acad. Sci. U.S.A.*, 107, 6652–6657,  
1340 <https://doi.org/10.1073/pnas.0908905107>, 2010.
- 1341 Sander, R., Keene, W. C., Pszenny, A. a. P., Arimoto, R., Ayers, G. P., Baboukas, E., Cainey, J. M., Crutzen, P. J., Duce, R. A.,  
1342 Hönninger, G., Huebert, B. J., Maenhaut, W., Mihalopoulos, N., Turekian, V. C., and Van Dingenen, R.: Inorganic bromine in  
1343 the marine boundary layer: a critical review, *Atmospheric Chemistry and Physics*, 3, 1301–1336, <https://doi.org/10.5194/acp-3-1301-2003>, 2003.
- 1345 Šantl-Temkiv, T., Gosewinkel, U., Starnawski, P., Lever, M., and Finster, K.: Aeolian dispersal of bacteria in southwest  
1346 Greenland: their sources, abundance, diversity and physiological states, *FEMS Microbiol Ecol*, 94,  
1347 <https://doi.org/10.1093/femsec/fiy031>, 2018.
- 1348 Šantl-Temkiv, T., Amato, P., Casamayor, E. O., Lee, P. K. H., and Pointing, S. B.: Microbial ecology of the atmosphere, *FEMS*  
1349 *Microbiology Reviews*, 46, fuac009, <https://doi.org/10.1093/femsre/fuac009>, 2022.
- 1350 Schartau, M., Engel, A., Schröter, J., Thoms, S., Völker, C., and Wolf-Gladrow, D.: Modelling carbon overconsumption and the  
1351 formation of extracellular particulate organic carbon, *Biogeosciences*, 4, 433–454, <https://doi.org/10.5194/bg-4-433-2007>,  
1352 2007.
- 1353 Schill, S. R., Burrows, S. M., Hasenecz, E. S., Stone, E. A., and Bertram, T. H.: The Impact of Divalent Cations on the Enrichment  
1354 of Soluble Saccharides in Primary Sea Spray Aerosol, *Atmosphere*, 9, 476, <https://doi.org/10.3390/atmos9120476>, 2018.
- 1355 Schmale, J., Zieger, P., and Ekman, A. M. L.: Aerosols in current and future Arctic climate, *Nature Climate Change*, 11, 95–105,  
1356 <https://doi.org/10.1038/s41558-020-00969-5>, 2021.
- 1357 Schmale, J., Sharma, S., Decesari, S., Pernov, J., Massling, A., Hansson, H.-C., von Salzen, K., Skov, H., Andrews, E., Quinn, P.  
1358 K., Upchurch, L. M., Eleftheriadis, K., Traversi, R., Gilardoni, S., Mazzola, M., Laing, J., and Hopke, P.: Pan-Arctic seasonal cycles  
1359 and long-term trends of aerosol properties from 10 observatories, *Atmospheric Chemistry and Physics*, 22, 3067–3096,  
1360 <https://doi.org/10.5194/acp-22-3067-2022>, 2022.
- 1361 Sharma, S., Barrie, L. a., Magnusson, E., Brattström, G., Leaitch, W. r., Steffen, A., and Landsberger, S.: A Factor and Trends  
1362 Analysis of Multidecadal Lower Tropospheric Observations of Arctic Aerosol Composition, Black Carbon, Ozone, and Mercury  
1363 at Alert, Canada, *Journal of Geophysical Research: Atmospheres*, 124, 14133–14161, <https://doi.org/10.1029/2019JD030844>,  
1364 2019.
- 1365 Shestakova, A., Chechin, D., Lüpkes, C., Hartmann, J., and Maturilli, M.: Foehn effect during easterly flow over Svalbard,  
1366 <https://doi.org/10.5194/acp-2021-478>, 2021.
- 1367 Simon, D. J., Hartmann, J., Schaefer, J., Zeppenfeld, S., Lüpkes, C., Hartmann, M., Wetzel, B., Heinold, B., Jurányi, Z., Schulz,  
1368 A., Köhler, L., Jörss, A.-M., Herber, A., Henning, S., Pöhlker, M. L., Roberts, G. C., and Stratmann, F.: Turbulent aerosol fluxes  
1369 from airborne measurements over the Arctic Ocean, *Geophys. Res. Lett.*, 52, e2025GL117094,  
1370 <https://doi.org/10.1029/2025GL117094>, 2025
- 1371 Sinreich, R., Coburn, S., Dix, B., and Volkamer, R.: Ship-based detection of glyoxal over the remote tropical Pacific Ocean,  
1372 *Atmospheric Chemistry and Physics*, 10, 11359–11371, <https://doi.org/10.5194/acp-10-11359-2010>, 2010.
- 1373 Sorooshian, A., Lu, M.-L., Brechtel, F. J., Jonsson, H., Feingold, G., Flagan, R. C., and Seinfeld, J. H.: On the Source of Organic  
1374 Acid Aerosol Layers above Clouds, *Environ. Sci. Technol.*, 41, 4647–4654, <https://doi.org/10.1021/es0630442>, 2007.
- 1375 Stein, A. F., Draxler, R. R., Rolph, G. D., Stunder, B. J. B., Cohen, M. D., and Ngan, F.: NOAA's HYSPLIT Atmospheric Transport  
1376 and Dispersion Modeling System, *Bull. Amer. Meteor. Soc.*, 96, 2059–2077, <https://doi.org/10.1175/BAMS-D-14-00110.1>,  
1377 2015.
- 1378 Struthers, H., Ekman, A. M. L., Glantz, P., Iversen, T., Kirkevåg, A., Mårtensson, E. M., Seland, Ø., and Nilsson, E. D.: The effect  
1379 of sea ice loss on sea salt aerosol concentrations and the radiative balance in the Arctic, *Atmospheric Chemistry and Physics*,  
1380 11, 3459–3477, <https://doi.org/10.5194/acp-11-3459-2011>, 2011.
- 1381 Su, B., Bi, X., Zhang, Z., Liang, Y., Song, C., Wang, T., Hu, Y., Li, L., Zhou, Z., Yan, J., Wang, X., and Zhang, G.: Enrichment of  
1382 calcium in sea spray aerosol: insights from bulk measurements and individual particle analysis during the R/V *Xuelong* cruise  
1383 in the summertime in Ross Sea, Antarctica, *Atmospheric Chemistry and Physics*, 23, 10697–10711,  
1384 <https://doi.org/10.5194/acp-23-10697-2023>, 2023.
- 1385 Theodosi, C., Im, U., Bougiatioti, A., Zarmas, P., Yenigun, O., and Mihalopoulos, N.: Aerosol chemical composition over  
1386 Istanbul, *Science of The Total Environment*, 408, 2482–2491, <https://doi.org/10.1016/j.scitotenv.2010.02.039>, 2010.

1387 Thyng, K., Greene, C. A., Hetland, R. D., Zimmerle, H. M., and DiMarco, S.: True colors of oceanography: Guidelines for effective  
1388 and accurate colormap selection, *Oceanography*, 3, <https://doi.org/10.5670/oceanog.2016.66>, 2016.

1389 Tilgner, A. and Herrmann, H.: Radical-driven carbonyl-to-acid conversion and acid degradation in tropospheric aqueous  
1390 systems studied by CAPRAM, *Atmospheric Environment*, 44, 5415–5422, <https://doi.org/10.1016/j.atmosenv.2010.07.050>,  
1391 2010.

1392 Tørseth, K., Aas, W., Breivik, K., Fjæraa, A. M., Fiebig, M., Hjellbrekke, A. G., Lund Myhre, C., Solberg, S., and Yttri, K. E.:  
1393 Introduction to the European Monitoring and Evaluation Programme (EMEP) and observed atmospheric composition change  
1394 during 1972–2009, *Atmospheric Chemistry and Physics*, 12, 5447–5481, <https://doi.org/10.5194/acp-12-5447-2012>,  
1395 2012.

1396 Trainic, M., Koren, I., Sharoni, S., Frada, M., Segev, L., Rudich, Y., and Vardi, A.: Infection Dynamics of a Bloom-Forming Alga  
1397 and Its Virus Determine Airborne Coccolith Emission from Seawater, *iScience*, 6, 327–335,  
1398 <https://doi.org/10.1016/j.isci.2018.07.017>, 2018.

1399 Triesch, N., van Pinxteren, M., Engel, A., and Herrmann, H.: Concerted measurements of free amino acids at the Cabo Verde  
1400 islands: high enrichments in submicron sea spray aerosol particles and cloud droplets, *Atmospheric Chemistry and Physics*,  
1401 21, 163–181, <https://doi.org/10.5194/acp-21-163-2021>, 2021.

1402 Turekian, V. C., Macko, S. A., and Keene, W. C.: Concentrations, isotopic compositions, and sources of size-resolved,  
1403 particulate organic carbon and oxalate in near-surface marine air at Bermuda during spring, *Journal of Geophysical Research: Atmospheres*,  
1404 108, <https://doi.org/10.1029/2002JD002053>, 2003.

1405 Veron, F.: Ocean Spray, *Annual Review of Fluid Mechanics*, 47, 507–538, <https://doi.org/10.1146/annurev-fluid-010814-014651>, 2015.

1407 Vihtakari, M.: PlotSvalbard: PlotSvalbard-Plot research data from Svalbard on maps, R package version 0.9.2, 2020.

1408 Warneck, P.: In-cloud chemistry opens pathway to the formation of oxalic acid in the marine atmosphere, *Atmospheric  
1409 Environment*, 37, 2423–2427, [https://doi.org/10.1016/S1352-2310\(03\)00136-5](https://doi.org/10.1016/S1352-2310(03)00136-5), 2003.

1410 Wendisch, M., Brückner, M., Burrows, J. P., Crewell, S., Dethloff, K., Ebell, K., Lüpkes, C., Macke, A., Notholt, J., and Quaas, J.:  
1411 Understanding causes and effects of rapid warming in the Arctic, *Eos*, 98, 2017.

1412 [Wendisch, M., Macke, A., Ehrlich, A., Lüpkes, C., Mech, M., Chechin, D., Dethloff, K., Barrientos, C., Bozem, H., Brückner, M.,  
1413 Clemen, H.-C., Crewell, S., Donth, T., Dupuy, R., Ebell, K., Egerer, U., Engelmann, R., Engler, C., Eppers, O., Gehrman, M.,  
1414 Gong, X., Gottschalk, M., Gourbeyre, C., Griesche, H., Hartmann, J., Hartmann, M., Heinold, B., Herber, A., Herrmann, H.,  
1415 Heygster, G., Hoor, P., Jafariserajehlou, S., Jäkel, E., Järvinen, E., Jourdan, O., Kästner, U., Kecorius, S., Knudsen, E. M., Köllner,  
1416 F., Kretzschmar, J., Lelli, L., Leroy, D., Maturilli, M., Mei, L., Mertes, S., Mioche, G., Neuber, R., Nicolaus, M., Nomokonova, T.,  
1417 Notholt, J., Palm, M., van Pinxteren, M., Quaas, J., Richter, P., Ruiz-Donoso, E., Schäfer, M., Schmieder, K., Schnaiter, M.,  
1418 Schneider, J., Schwarzenböck, A., Seifert, P., Shupe, M. D., Siebert, H., Spreen, G., Stapf, J., Stratmann, F., Vogl, T., Weltj, A.,  
1419 Wex, H., Wiedensohler, A., Zanatta, M., and Zeppenfeld, S.: The Arctic Cloud Puzzle: Using ACLOUD/PASCAL Multi-Platform  
1420 Observations to Unravel the Role of Clouds and Aerosol Particles in Arctic Amplification, \*Bull. Amer. Meteor. Soc.\*,  
1421 <https://doi.org/10.1175/BAMS-D-18-0072.1>, 2018.](#)

1422 Wendisch, M., Brückner, M., Crewell, S., Ehrlich, A., Notholt, J., Lüpkes, C., Macke, A., Burrows, J. P., Rinke, A., Quaas, J.,  
1423 Maturilli, M., Schemann, V., Shupe, M. D., Akansu, E. F., Barrientos-Velasco, C., Bärfuss, K., Blechschmidt, A.-M., Block, K.,  
1424 Bougoudis, I., Bozem, H., Böckmann, C., Bracher, A., Bresson, H., Bretschneider, L., Buschmann, M., Chechin, D. G., Chylik, J.,  
1425 Dahlke, S., Deneke, H., Dethloff, K., Donth, T., Dorn, W., Dupuy, R., Ebell, K., Egerer, U., Engelmann, R., Eppers, O., Gerdes, R.,  
1426 Gierens, R., Gorodetskaya, I. V., Gottschalk, M., Griesche, H., Gryanik, V. M., Handorf, D., Harm-Altstädter, B., Hartmann, J.,  
1427 Hartmann, M., Heinold, B., Herber, A., Herrmann, H., Heygster, G., Höschel, I., Hofmann, Z., Hölemann, J., Hünerbein, A.,  
1428 Jafariserajehlou, S., Jäkel, E., Jacobi, C., Janout, M., Jansen, F., Jourdan, O., Jurányi, Z., Kalesse-Los, H., Kanzow, T., Kätner,  
1429 R., Kliesch, L. L., Klingebiel, M., Knudsen, E. M., Kovács, T., Körtke, W., Krampe, D., Kretzschmar, J., Kreyling, D., Kulla, B.,  
1430 Kunkel, D., Lampert, A., Lauer, M., Lelli, L., Lerber, A. von Linke, O., Löhnert, U., Lonardi, M., Losa, S. N., Losch, M., Maahn,  
1431 M., Mech, M., Mei, L., Mertes, S., Metzner, E., Mewes, D., Michaelis, J., Mioche, G., Moser, M., Nakoudi, K., Neggers, R.,  
1432 Neuber, R., Nomokonova, T., Oelker, J., Papakonstantinou-Presvelou, I., et al.: Atmospheric and Surface Processes, and  
1433 Feedback Mechanisms Determining Arctic Amplification: A Review of First Results and Prospects of the (AC)3 Project, *Bulletin  
1434 of the American Meteorological Society*, 104, E208–E242, <https://doi.org/10.1175/BAMS-D-21-0218.1>, 2023.

1435 White, W. H.: Chemical markers for sea salt in IMPROVE aerosol data, *Atmospheric Environment*, 42, 261–274,  
1436 <https://doi.org/10.1016/j.atmosenv.2007.09.040>, 2008.

1437 Wickham, H.: Reshaping Data with the reshape Package, *Journal of Statistical Software*, 21, 1–20, 2007.

1438 Wickham, H.: ggplot2: Elegant Graphics for Data Analysis, Springer-Verlag New York, [https://doi.org/10.1007/978-3-319-24277-4\\_2](https://doi.org/10.1007/978-3-319-24277-4_2), 2016.

1440 Wickham, H., François, R., Henry, L., Müller, K., and Vaughan, D.: dplyr: A Grammar of Data Manipulation, R package version  
1441 1.1.4, 2023a.

1442 Wickham, H., Pedersen, T. L., and Seidel, D.: scales: Scale Functions for Visualization, R package version 1.3.0, 2023b.

Formatiert: Abstand Nach: 6 Pt.

- 1443 Wietz, M., Engel, A., Ramondenc, S., Niwano, M., von Appen, W.-J., Priest, T., von Jackowski, A., Metfies, K., Bienhold, C., and  
 1444 Boetius, A.: The Arctic summer microbiome across Fram Strait: Depth, longitude, and substrate concentrations structure  
 1445 microbial diversity in the euphotic zone, *Environmental Microbiology*, 26, e16568, <https://doi.org/10.1111/1462-2920.16568>, 2024.
- 1447 Wietz, M., van Pinxteren, M., Freese, H. M., Sproer, C., and Zeppenfeld, S.: Seasonal connectivity of microbes and  
 1448 carbohydrates between ocean, atmosphere, and cryosphere in Kongsfjorden (Svalbard, Arctic Ocean), preprint,  
 1449 <https://doi.org/10.64898/2025.12.01.691664>, uploaded on 2 December 2025.
- 1450 Willis, M. D., Leaitch, W. R., and Abbatt, J. P. D.: Processes Controlling the Composition and Abundance of Arctic Aerosol,  
 1451 *Reviews of Geophysics*, 56, 621–671, <https://doi.org/10.1029/2018RG000602>, 2018.
- 1452 Wong, J. P. S., Tsagkaraki, M., Tsiotra, I., Mihalopoulos, N., Violaki, K., Kanakidou, M., Sciare, J., Nenes, A., and Weber, R. J.:  
 1453 Effects of Atmospheric Processing on the Oxidative Potential of Biomass Burning Organic Aerosols, *Environ. Sci. Technol.*, 53,  
 1454 6747–6756, <https://doi.org/10.1021/acs.est.9b01034>, 2019.
- 1455 Wurl, O. and Holmes, M.: The gelatinous nature of the sea-surface microlayer, *Marine Chemistry*, 110, 89–97,  
 1456 <https://doi.org/10.1016/j.marchem.2008.02.009>, 2008.
- 1457 Xu, W., Ovadnevaite, J., Fossom, K. N., Lin, C., Huang, R.-J., Ceburnis, D., and O'Dowd, C.: Sea spray as an obscured source for  
 1458 marine cloud nuclei, *Nat. Geosci.*, 15, 282–286, <https://doi.org/10.1038/s41561-022-00917-2>, 2022.
- 1459 Yang, C., Zhou, S., Zhang, C., Yu, M., Cao, F., and Zhang, Y.: Atmospheric Chemistry of Oxalate: Insight Into the Role of Relative  
 1460 Humidity and Aerosol Acidity From High-Resolution Observation, *Journal of Geophysical Research: Atmospheres*, 127,  
 1461 e2021JD035364, <https://doi.org/10.1029/2021JD035364>, 2022.
- 1462 Yttri, K. E., Bäcklund, A., Conen, F., Eckhardt, S., Evangeliou, N., Fiebig, M., Kasper-Giebl, A., Gold, A., Gundersen, H., Myhre,  
 1463 C. L., Platt, S. M., Simpson, D., Surratt, J. D., Szidat, S., Rauber, M., Tørseth, K., Ytre-Eide, M. A., Zhang, Z., and Aas, W.:  
 1464 Composition and sources of carbonaceous aerosol in the European Arctic at Zeppelin Observatory, Svalbard (2017 to 2020),  
 1465 *Atmospheric Chemistry and Physics*, 24, 2731–2758, <https://doi.org/10.5194/acp-24-2731-2024>, 2024.
- 1466 Yu, H., Kaufman, Y. J., Chin, M., Feingold, G., Remer, L. A., Anderson, T. L., Balkanski, Y., Bellouin, N., Boucher, O., Christopher,  
 1467 S., DeCola, P., Kahn, R., Koch, D., Loeb, N., Reddy, M. S., Schulz, M., Takemura, T., and Zhou, M.: A review of measurement-  
 1468 based assessments of the aerosol direct radiative effect and forcing, *Atmospheric Chemistry and Physics*, 6, 613–666,  
 1469 <https://doi.org/10.5194/acp-6-613-2006>, 2006.
- 1470 Zäncker, B., Cunliffe, M., and Engel, A.: Eukaryotic community composition in the sea surface microlayer across an east–west  
 1471 transect in the Mediterranean Sea, *Biogeosciences*, 18, 2107–2118, <https://doi.org/10.5194/bg-18-2107-2021>, 2021.
- 1472 [Zeising, M., Oziel, L., Thoms, S., Gürses, Ö., Hauck, J., Heinold, B., Losa, S. N., van Pinxteren, M., Völker, C., Zeppenfeld, S., and  
 1473 Bracher, A.: Assessment of transparent exopolymer particles in the Arctic Ocean implemented into the coupled ocean–sea  
 1474 ice–biogeochemistry model FESOM2.1–RECoM3, \*Geoscientific Model Development\*, 19, 2077–2109,  
 1475 <https://doi.org/10.5194/gmd-19-2077-2026>, 2026.](https://doi.org/10.5194/gmd-19-2077-2026)
- 1476 Zeppenfeld, S. and Schmidt, L.: Dissolved and particulate carbohydrates and inorganic ions in the sea surface microlayer and  
 1477 bulk water of Kongsfjorden (Autumn 2021/Spring 2022), <https://doi.org/10.1594/PANGAEA.982606>, 2025.
- 1478 Zeppenfeld, S., van Pinxteren, M., Engel, A., and Herrmann, H.: A protocol for quantifying mono- and polysaccharides in  
 1479 seawater and related saline matrices by electro-dialysis (ED) – combined with HPAEC-PAD, *Ocean Science*, 16, 817–830,  
 1480 <https://doi.org/10.5194/os-16-817-2020>, 2020.
- 1481 Zeppenfeld, S., van Pinxteren, M., van Pinxteren, D., Wex, H., Berdalet, E., Vaqué, D., Dall'Osto, M., and Herrmann, H.: Aerosol  
 1482 Marine Primary Carbohydrates and Atmospheric Transformation in the Western Antarctic Peninsula, *ACS Earth Space Chem.*,  
 1483 5, 1032–1047, <https://doi.org/10.1021/acsearthspacechem.0c00351>, 2021.
- 1484 Zeppenfeld, S., van Pinxteren, M., Hartmann, M., Zeising, M., Bracher, A., and Herrmann, H.: Marine carbohydrates in Arctic  
 1485 aerosol particles and fog – diversity of oceanic sources and atmospheric transformations, *Atmospheric Chemistry and Physics*,  
 1486 23, 15561–15587, <https://doi.org/10.5194/acp-23-15561-2023>, 2023.
- 1487 Zeppenfeld, S., Schaefer, J., van Pinxteren, M., and Schmidt, L.: Marine combined carbohydrates and inorganic ions in  
 1488 atmospheric total suspended particles across altitudes in the lower troposphere of Ny-Ålesund, Svalbard,  
 1489 <https://doi.org/10.1594/PANGAEA.982703>, 2025.
- 1490 Zhou, S., Gonzalez, L., Leithead, A., Finewax, Z., Thalman, R., Vlasenko, A., Vagle, S., Miller, L. A., Li, S.-M., Bureekul, S.,  
 1491 Furutani, H., Uematsu, M., Volkamer, R., and Abbatt, J.: Formation of gas-phase carbonyls from heterogeneous oxidation of  
 1492 polyunsaturated fatty acids at the air–water interface and of the sea surface microlayer, *Atmospheric Chemistry and Physics*,  
 1493 14, 1371–1384, <https://doi.org/10.5194/acp-14-1371-2014>, 2014.
- 1494 Zhu, B., Sun-Waterhouse, D., and You, L.: Insights into the mechanisms underlying the degradation of xylooligosaccharides in  
 1495 UV/H<sub>2</sub>O<sub>2</sub> system, *Carbohydrate Polymers*, 317, 121091, <https://doi.org/10.1016/j.carbpol.2023.121091>, 2023.

Formatiert: Abstand Nach: 12 Pt.

1496 Zhu, Y.-S., Connolly, A., Guyon, A., and FitzGerald, R. J.: Solubilisation of calcium and magnesium from the marine red algae  
1497 Lithothamnion calcareum, International Journal of Food Science and Technology, 49, 1600–1606,  
1498 <https://doi.org/10.1111/ijfs.12459>, 2014.